



HAL
open science

Persistent anticyclonic conditions and climate change exacerbated the exceptional 2022 European-Mediterranean drought

Davide Faranda, Salvatore Pascale, Burak Bulut

► **To cite this version:**

Davide Faranda, Salvatore Pascale, Burak Bulut. Persistent anticyclonic conditions and climate change exacerbated the exceptional 2022 European-Mediterranean drought. *Environmental Research Letters*, inPress. hal-03907855v1

HAL Id: hal-03907855

<https://hal.science/hal-03907855v1>

Submitted on 20 Dec 2022 (v1), last revised 24 Mar 2023 (v3)

HAL is a multi-disciplinary open access archive for the deposit and dissemination of scientific research documents, whether they are published or not. The documents may come from teaching and research institutions in France or abroad, or from public or private research centers.

L'archive ouverte pluridisciplinaire **HAL**, est destinée au dépôt et à la diffusion de documents scientifiques de niveau recherche, publiés ou non, émanant des établissements d'enseignement et de recherche français ou étrangers, des laboratoires publics ou privés.

Persistent anticyclonic conditions and climate change exacerbated the exceptional 2022 European-Mediterranean drought

Daive Faranda^{1,2,3,*}, Salvatore Pascale^{4,5,*}, Burak Bulut^{1,*}

¹ Laboratoire des Sciences du Climat et de l'Environnement, UMR 8212 CEA-CNRS-UVSQ, Université Paris-Saclay & IPSL, CE Saclay l'Orme des Merisiers, 91191, Gif-sur-Yvette, France

² London Mathematical Laboratory, 8 Margravine Gardens, London, W6 8RH, British Islands

³ LMD-IPSL, Ecole Polytechnique, Institut Polytechnique de Paris, ENS, PSL Research University, Sorbonne Université, CNRS, Palaiseau, France

⁴ University of Bologna, Department of Physics and Astronomy, Bologna, Italy

⁵ Centre for Sustainability and Climate Change, Bologna Business School, Bologna, Italy

* All authors have equally contributed to this work

E-mail: davide.faranda@cea.fr, salvatore.pascale@unibo.it, burak.bulut@cea.fr

20 December 2022

Abstract. A prolonged drought affected Western Europe and the Mediterranean region in the first nine months of 2022 producing large socio-ecological impacts. The role of anthropogenic climate change (ACC) in exacerbating this drought has been often invoked in the public debate, but the link between atmospheric circulation and ACC has not received much attention so far. Here we address this question by applying the method of circulation analogs, which allows us to identify atmospheric patterns in the period 1836-2021 very similar to those occurred in 2022. By comparing the circulation analogs when global warming was absent (1836-1915) with those occurred recently (1942-2021), and by excluding interannual and interdecadal variability as possible drivers, we identify the contribution of ACC. The 2022 drought was associated with an anticyclonic anomaly over Western Europe persistent over December 2021-August 2022. Circulation analogs of this atmospheric pattern in 1941-2021 feature 500 hPa geopotential height anomalies larger in both extent and magnitude, and higher temperatures at the surface, relative to those in 1836-1915. Both factors exacerbated the drought, by increasing the area affected and enhancing soil drying through evapotranspiration. While the occurrence of the atmospheric circulation associated with the 2022 drought has not become more frequent in recent decades, there is an increase of its interdecadal variability for which the influence of the Atlantic Multidecadal oscillation cannot be ruled-out.

Keywords: Drought - Climate Change - Attribution

1. Characteristics of the 2022 Euro-Mediterranean drought

Intense and prolonged drought conditions affected large portions of France, Italy, and Spain throughout most of 2022. The drought, related to a persistent lack of precipitation in the last months of 2021, became evident in northwestern Italy since March 2022 [1] and then expanded to western Europe in the following months. The severity of the drought then further worsened during spring and summer 2022 (Fig. 1b), due to a persistent lack of precipitation combined with a sequence of heatwaves from May onwards [2, 3] which further dried the soil through enhanced evapotranspiration [4]. Fig. 1c,d shows record-breaking negative values of the drought indicator SPEI9 in August 2022 (see Sect. 2.1 for details about SPEI) over the last seventy years, over southern France and Northern Italy. The area-average of SPEI9 over the two areas was consistently below -2 (extreme drought), with local grid points having SPEI9 values below -3.

The socio-ecological impacts of the 2022 drought have been severe in Italy, France and Spain. The exceptionality of the water and heat stress substantially reduced yields of some of the main crops like, e.g., grain maize, soybean, and sunflowers, with reductions of around 15% relative to the last 5-year average [5]. In Italy, about 50% of the population was affected by the drought emergency water restrictions, especially in the North of the country. The Po river basin Authority reported record-breaking levels of inland salt intrusion from the Po delta up to 40 km from the sea coast. Reduced stored water severely impacted the energy sector for both hydropower generation and cooling systems of other power plants in the north of the country. In southern France, wildfires associated with the extreme drought conditions were also more widespread, with a surface of burned land more than double than in 2021 and about 4.6 times the average of the period 2012-2021. Sixty-six French “departments” were at the highest drought warning level in August, with at least ninety-three departments at one of the top three levels of warning for drought. Similar impacts on agriculture, energy production and domestic water usage were reported in Spain, Portugal and Netherlands too [2].

While drought is a complex phenomenon [6, 7], whose intensity can be exacerbated by non-trivial land surface-atmosphere feedbacks and land usage [8], the large scale atmospheric circulation played a key role in driving the 2022 Euro-Mediterranean drought. This is evident when examining the circulation anomalies during the first eight months of 2022: a persistent high pressure anomaly centered over France is visible both in the lower and middle troposphere (Fig. 1a). This circulation anomaly favored meteorological conditions characterized by stable conditions with no precipitation over large swaths of Europe.

The 2022 Euro-Mediterranean drought unfolded as El Niño-Southern Oscillation (ENSO) was in a persistent negative phase (La Niña) since the summer of 2020. It is therefore natural to ask whether La Niña did play a role in remotely driving the long-lasting anticyclonic circulation. The relationship between ENSO and the North Atlantic-European sector is not as well defined as for other regions of the world, and probably non-stationary in time [9, 10, 11]. If we compare the slow-evolving circulation

42 anomaly of 2022 in Europe with that of other years featuring similar 3-year La Niña
43 conditions (i.e., 1956, 1975, and 2000), we see large differences in the intensity and
44 spatial patterns of the anomalies and no resemblance to the 2022 pattern (Fig. S1).
45 This leads us to conjecture that there might not be a simple causality relationship
46 between La Niña and the persistent anticyclonic anomaly observed over western Europe
47 in 2022, although this is a point that we will further investigate in this study.

48 The 2022 drought had large societal impacts rising the attention of the media at
49 the national and international level [12, 13, 14, 3] and putting water management high
50 on the agenda of water managers and decision-makers. Questions on the role played
51 by the ongoing anthropogenic climate change (ACC) on this drought, and eventually
52 on future droughts, are therefore pressing in the media debate, and answers to these
53 questions are urgent to manage future similar water crises. Specifically, the questions we
54 ask here are: how rare was the prolonged atmospheric circulation anomaly that drove
55 the 2022 drought situation? Was such anomaly changed in shape, intensity, and thermal
56 structure because of ACC, thus exacerbating similar drought events?

57 In this study, we address these questions through the method of the analogs of
58 circulation for extreme event attribution [15, 16]. We use the implementation developed
59 by [17] for short-lived meteorological events of a few days of duration (e.g., cyclones, hot
60 and cold spells, etc.), which we adapt to account for long-lasting events such as droughts.
61 For the construction of factual and counterfactual climate [18], we rely on long-term
62 monthly reanalyses (1836 to present) that allow for the construction of robust statistics.
63 We, therefore, compare analogs of this averaged circulation in factual (1836-1915) and
64 counterfactual (1941-2021) periods and study the associated temperature, precipitation,
65 and SPEI9, looking for statistically significant differences that can then be attributed
66 to climate change. Other complementary approaches for event attribution of extreme
67 drought rely on single model initial-condition large ensembles [19, 20, 21]. While a
68 model ensemble approach allows for a separation of counterfactual vs factual climate,
69 it still suffers from model biases that can limit the realism of the results. Therefore in
70 this study, we focus on observations only, planning to analyze models as a second step.

71 2. Methods and Data

72 2.1. Drought and circulation variables

73 We use the Standardized Precipitation Evapotranspiration Index aggregated at 9 months
74 (SPEI9) to monitor and characterize the 2022 drought [4, 22]. The SPEI generalizes the
75 Standard Precipitation Index (SPI, [23]) by taking into account surface temperature too
76 through its effects on Potential Evapotranspiration. It has been demonstrated that high
77 temperatures - typical of, e.g., heat waves - increase drought stress under precipitation
78 shortages by dramatically increasing evapotranspiration [24]. The SPEI9 is calculated
79 first by estimating the difference between precipitation and potential evapotranspiration
80 at the surface, which provides a simple measure of the water deficit or surplus, and then

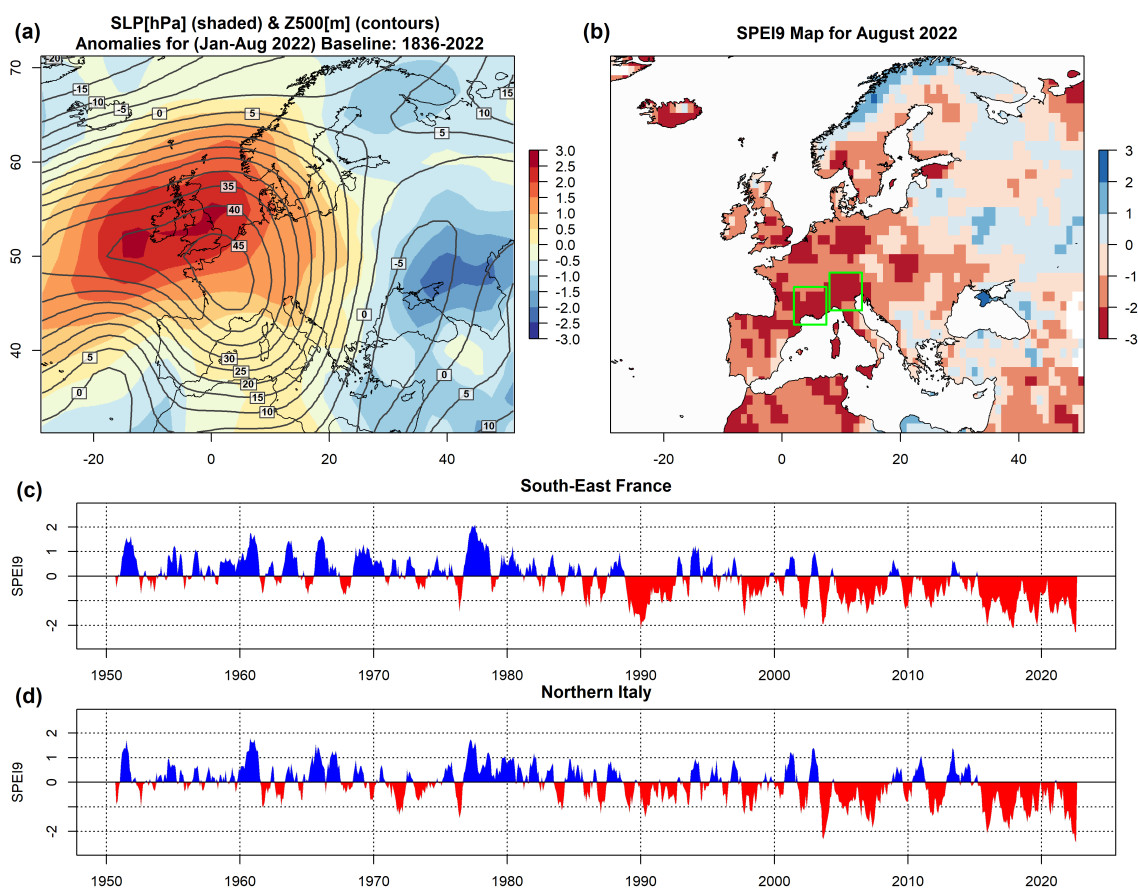


Figure 1. Characteristics of the 2022 European drought. (a) 2022 January-to-August anomalies of 500 hPa geopotential height (contour interval -15 and 45 m) and Mean Sea Level Pressure (shading interval -3 and 3 hPa), (b) map of SPEI9 in August 2022, and (c,d) SPEI9 time series obtained as an average of grid points within the selected regions highlighted in green.

81 aggregating it at different time scales (SPEI1, SPEI3, SPEI6, etc.). Similarly to the
 82 SPI, the time scale of accumulation of the water deficits (e.g., 3 months, 6 months, 12
 83 months, etc.) is very important for practical reasons, as it differentiates meteorological
 84 droughts - typically of a few months' duration - from hydrological droughts, emerging
 85 at longer timescales (6 months or longer).

86 The large scale atmospheric circulation over the North Atlantic-European sector
 87 is investigated through the 500 hPa geopotential height (Z500) and sea level pressure
 88 (SLP). All Z500 and SLP data used in the analyses of the analogs of circulation are
 89 first detrended and then deseasonalized by subtracting, for each month, the 1836-2022
 90 monthly average. Details on these applied procedures can be found in the Supplementary
 91 Material and in Fig. S2. We use the 2-meter temperature to keep track of the impact of
 92 global warming, and the precipitation rate to further cross-checking drought conditions
 93 along with SPEI. We do not apply any preprocessing to 2-meter temperature, the

94 precipitation rate, and SPEI9. A list of the variables, and their symbols, used in this
 95 study is shown in Tab. [1](#)

96 2.2. Data

Table 1. Data sets used in the study, the period of record available, spatial resolution, and references.

Variable	Spatial Resolution	Temporal Coverage	Reference
SLP, Z500, PRATE, T2M	1° x 1°	01/1836-12/2015	NOAA/CIRES/DOE 20CRv3, (Slivinsk et al., 2019)
SLP, Z500	2.5° x 2.5°	01/1948-08/2022	NCEP/NCAR Reanalysis I, (Kalnay et al., 1996)
PRATE, T2M	1.875° x 1.90°	01/1979-08/2022	NCEP/DOE Reanalysis II, (Kanamitsu et al., 2002)
ENSO	1° x 1°	01/1870-08/2022	HadISST1 Nino3.4 Index, (Rayner et al., 2003)
AMO	1° x 1°	01/1850-08/2022	Atlantic Multidecadal Variability index, (van Oldenborgh et al., 2009)
SPEI9	1° x 1°	01/1950-08/2022	SPEI9Global Drought Monitor, (Beguería et al., 2014)

97 Values of SPEI9 are obtained from the SPEI Global Drought Monitor, freely
 98 available at <https://spei.csic.es/index.html> at 1°×1° horizontal resolution from
 99 1950 to present. The SPEI Global Drought Monitor offers near real-time SPEI estimates
 100 at various temporal scales (SPEI1, SPEI3, etc.) at the global scale, based on the
 101 NOAA NCEP CPC GHCN_CAMS gridded dataset for mean temperature and the Global
 102 Precipitation Climatology Centre for the monthly precipitation data. The CPC data
 103 with an original resolution of 0.5°, is interpolated to the resolution of 1°.

104 To capture the 2022 drought condition, we use SPEI9 as the 9-month aggregation
 105 timescale roughly corresponds to the period of negative rain deficit observed over western
 106 Europe. To analyze the atmospheric circulation over the North Atlantic-European
 107 sector and their relationship to the drought, we use the 20CRv3 reanalyses [\[25\]](#). The
 108 choice of 20CRv3 - which spans the period 1836-2015 and it is available at 1°×1°
 109 horizontal resolution - is dictated by the need of having a century-long reanalysis
 110 product that can thus provide more reliable statistics with regards to rare events, as
 111 in the case of intense droughts, and a sufficient number of analogs of the atmospheric
 112 circulation anomaly associated with the 2022 drought. In order to cover the most recent
 113 years and the 2022 drought event, we complement 20CRv3 for the period January
 114 2016-August 2022 with NCEP reanalysis [\[26\]](#). We use both the NCEP/DOE and

115 NCEP/NCAR reanalyses (Table 1). 20CRv3 and NCEP Reanalysis data are freely
116 available at <https://psl.noaa.gov/data/gridded>. In order to eliminate differences
117 between 20CRv3 and NCEP reanalysis datasets, we applied a bias correction to the
118 complementary period (after 2016) where datasets are obtained from NCEP reanalysis.
119 Details of how we combined the two datasets as well as how bias corrections are
120 performed are provided in the Supplementary Material and in Fig. S3. SPEI9 is
121 calculated for the combined reanalyses 20CRv3 and NCEP by using the R package
122 SPEI9 [22]. This tool assumes a log-logistic probability distribution [4] calibrated for
123 20CRv3 using all available years.

124 We evaluate the effect of interannual and interdecadal variability on the 2022
125 drought and on past analog droughts using the ENSO3.4 index for ENSO (1870 -
126 present) and the Atlantic Multidecadal Oscillation (AMO, 1850 - present) monthly
127 indices computed from the HadISST1 data and retrieved from KNMI's climate explorer
128 www.climexp.knmi.nl. Missing values are replaced by NaN and not counted in the
129 analysis. We remark that NaN values represent only less or at most about 10% of the
130 total data. In particular, the ENSO3.4 index is as defined by [27] and the AMO index
131 is computed as described in [28].

132 2.3. Analogs attribution method

133 The attribution method we use here is described in detail in [17], where it has been
134 applied and validated for daily SLP maps associated with a number of extreme events
135 occurred in 2021. In this study, we modify this method, born to deal with extreme events
136 of the duration of a few days, in order to apply it to slow-evolving extreme events like
137 droughts, which can have a duration of several months. To isolate the slow-evolving
138 component of the atmospheric circulation (Fig. 1a) and for consistency with SPEI9, we
139 smooth Z500 and SLP by applying a nine-month backward moving average. We then
140 search for analogs of the SLP and Z500 anomalies observed in August 2022 (Fig. 1a)
141 in the factual period 1941-2021 and compare them to the analogs in the counterfactual
142 period 1836-1915. For each period, we examine all monthly averaged maps and select
143 the best 29 analogs, i.e. the maps minimizing the Euclidean distance to the event map
144 itself. The number of 29 corresponds approximately to the smallest 3‰ Euclidean
145 distances in each subset of our data. We tested the extraction of 15 to 30 analogous
146 maps, without finding qualitatively important differences in our results. For the factual
147 period, as is customary in attribution studies, the event itself is suppressed. In addition,
148 we prohibit the search for analogs in 2022.

149 Unlike attribution techniques based on a statistical analysis of meteorological
150 variables, conditioning to specific atmospheric circulation patterns via analogs allows
151 us to link attribution to the dynamics driving extreme events. In addition, the analogs
152 method allows us to determine when a weather event is unprecedented because of an
153 atmospheric circulation that has never been observed in the past, making it statistically
154 impossible to say whether climate change has made the event more likely. To account

155 for the possible influence of low-frequency modes of natural variability in explaining the
156 differences between the two periods, we also consider the possible roles of ENSO and
157 AMO.

158 Following [17], we introduce additional indicators that further support our
159 interpretation of analog-based results:

160 *2.3.1. Analog quality Q .* Q is the average Euclidean distance of a given circulation
161 pattern from its closest 33 analogs. One can then compare Q associated with the
162 extreme event to Q for each analog of the extreme event. If the value of Q for the
163 extreme event belongs to the same distribution of the values of Q for the analogs, then
164 the extreme event has good analogs. If instead the Q for the extreme event is larger than
165 that of the analogs, then the extreme event is associated with a very unusual circulation
166 pattern, and care must be taken in interpreting the results. Differences between the
167 counterfactual and factual periods in the value of Q associated with the extreme event
168 indicate whether the atmosphere is visiting states (analog) that are more or less similar
169 to the map associated with the extreme.

170 *2.3.2. Predictability Index D .* Using dynamical systems theory [29, 30, 31], we can
171 compute the local dimension D of each Z500 (SLP) map [32, 33]. The local dimension
172 is a proxy for the number of degrees of freedom of the field, meaning that the higher
173 D , the more unpredictable the temporal evolution of the Z500 (SLP) maps will be
174 [34, 35, 36]. If the dimension D of the extreme event analyzed is higher or lower than
175 that of its analogs, then the extreme will be respectively less or more predictable than
176 the closest dynamical situations identified in the data.

177 *2.3.3. Persistence index Θ .* Another quantity derived from dynamical systems theory
178 is the persistence Θ of a given configuration [37]. Persistence estimates the number of
179 subsequent months we are likely to observe a map that is an analog of the one under
180 consideration.

181 *2.3.4. Seasonality of analogs.* We can count the number of analogs per each month
182 to detect whether there has been a shift in circulation to months earlier or later in the
183 season. This can have strong thermodynamic implications, for example, if a circulation
184 leading to large positive temperature anomalies in early spring becomes more frequent
185 later in the season when average temperatures are much higher.

186 We compute the analog quality, the predictability index and the persistence index,
187 and their statistical distribution, for extreme events in the factual and counterfactual
188 world. Similarly, we estimate the persistence of the analogs for the two periods.

2.4. Association with ENSO and AMO

To account for the effect of natural interannual and interdecadal variability, we extract from the entire time series of the ENSO and AMO indices only the values in correspondence of “analog” months, for both the counterfactual and factual periods. If the two distributions – ENSO (AMO) during analogs in the counterfactual period and ENSO (AMO) during analogs in the factual period – do differ significantly between the two periods, then it is not possible to exclude that thermodynamic or dynamic differences in the analogs are partly due to these modes of natural variability, rather than anthropogenic forcing. On the other hand, if it is not possible to reject the null hypothesis of equal distributions, observed changes in analogs cannot be due to these two modes of natural variability and hence are attributed to human activity. It is worth noting that such null hypothesis of no influence of natural variability is coherent with the view of [38].

To assess the significance of changes in factual vs. counterfactual distributions, we conduct in all cases a two-sided Cramér-von Mises test at the 0.05 significance level. If the p-value is smaller than 0.05, the null hypothesis ($H = 0$) that the two samples come from the same distribution can be rejected [39].

3. Results

We perform the analogs attribution on both Z500 and SLP. Our results do not sensibly depend on the choice of the variable nor on the choice of applying or not the bias corrections to the reanalyses products (see Supplementary). Here we present the results for Z500 20CRv3 and DOE data with bias corrections, referring the reader for all other cases to the Supplementary Material.

3.1. Pattern analysis

Figure 2a shows the Z500 anomaly field averaged for the first 8 months of 2022. We note a dipolar structure of the Z500 anomaly, with positive values on Western Europe and negative on Eastern Europe, typical of Atlantic ridge patterns [40]. Analog for the counterfactual (Fig. 2b) and factual (Fig. 2c) periods show a similar dipolar structure. The difference between the analogs of the factual and counterfactual period, $\Delta Z500$, highlights statistically significant diversities between the two fields (Fig. 2d). In particular, the factual climate features a dipole structure with larger positive anomalies over western Europe relative to the counterfactual climate. Furthermore, the positive anomaly has a larger spatial extension and it extends further westward over the Atlantic and southeastward towards the Mediterranean basin. This feature is pretty robust and independent of the choice of variables (SLP vs. Z500) and reanalyses (Fig. S4-Fig. S10).

Fig. 2e shows T2M averaged over the first 9 months up to August 2022 while Fig. 2f-g show the average T2M associated with the two sets of analogs. The analysis for T2M shows that the temperature field of the 2022 drought (Fig. 2e) is exceptionally warmer

227 when compared to those associated with analogs of the counterfactual (Fig. 2f) or factual
228 (Fig. 2g) periods. The difference $\Delta T2M$ between the two is shown in (Fig. 2h) and it
229 shows an impressive warming associated with the Z500 analogs in the factual periods,
230 as we would somewhat expect due to the ongoing global warming [41]. Note that this
231 warming is way beyond the average global (1.2°C) but also regional warming and does
232 not include the event itself.

233 When comparing PRATE for the drought 2022 (Fig. 2i) with those associated with
234 counterfactual (Fig. 2j) and factual (Fig. 2k) analogs, we note some similarities such
235 as large precipitation amounts over the Alps, Norway, and southern Iceland, while the
236 western Atlantic is dryer in 2022 than in the analogs. Let us bear in mind that these
237 are precipitation estimates obtained from reanalyses and therefore do not have to be
238 considered as reliable as observations. While not accurate, they are still useful to connect
239 circulation and thermal anomalies to precipitation deficits and hence droughts. What is
240 more informative is the difference in PRATE associated with factual and counterfactual
241 analogs (Fig. 2l), which shows a tendency to drier conditions in the factual climate
242 relative to the counterfactual climate, with two minima over the British isles and over
243 the Mediterranean.

244 We complete this analysis by comparing the pattern of SPEI9 of August 2022
245 (Fig. 2m; see also Fig. 1b for an estimate of the same field based on observations)
246 with the typical SPEI9 patterns associated with the Z500 factual and counterfactual
247 analogs (Fig. 2n-Fig. 2o). When comparing the structure of SPEI9 from counterfactual
248 to factual period (Fig. 2p), we see an extension of the area with negative values from
249 Eastern Atlantic and the Iberian peninsula to all Western and Southern Europe. In
250 fact, the resulting difference $\Delta SPEI9$ shows a marked tendency to negative values
251 over all Europe. As SPEI9 takes into account both precipitation and surface potential
252 evapotranspiration – which is temperature dependent – this patterns is fully consistent
253 with both the tendency towards higher temperatures (Fig. 2h) and reduced precipitation
254 (Fig. 2l) of Z500 analogs in the factual climate.

255 3.2. Dynamical indicators analysis

256 An analysis of the analogs quality Q (Fig. 2q) shows that factual analogs, as compared
257 to counterfactual ones, are more similar to the Z500 pattern defined in Fig. 2a. This is
258 because the Euclidean distance of the 2022 circulation pattern from the factual analogs
259 (blue dots) is well centered with the distribution of the distances of 2022 analogs from
260 their analogs (pink violin plot). Contrary to that, the distance of the 2022 circulation
261 pattern from the counterfactual analogs is at the edge for the counterfactual (blue violin
262 plot). The difference is significant with p-value virtually zero. This indicates that,
263 although the frequency of occurrence of analogs patterns remains similar in factual and
264 counterfactual periods (see analysis in Sect. 3.3), the most recent (factual) patterns
265 have become more similar to that of 2022 (better quality) and therefore more prone to
266 generate droughts.

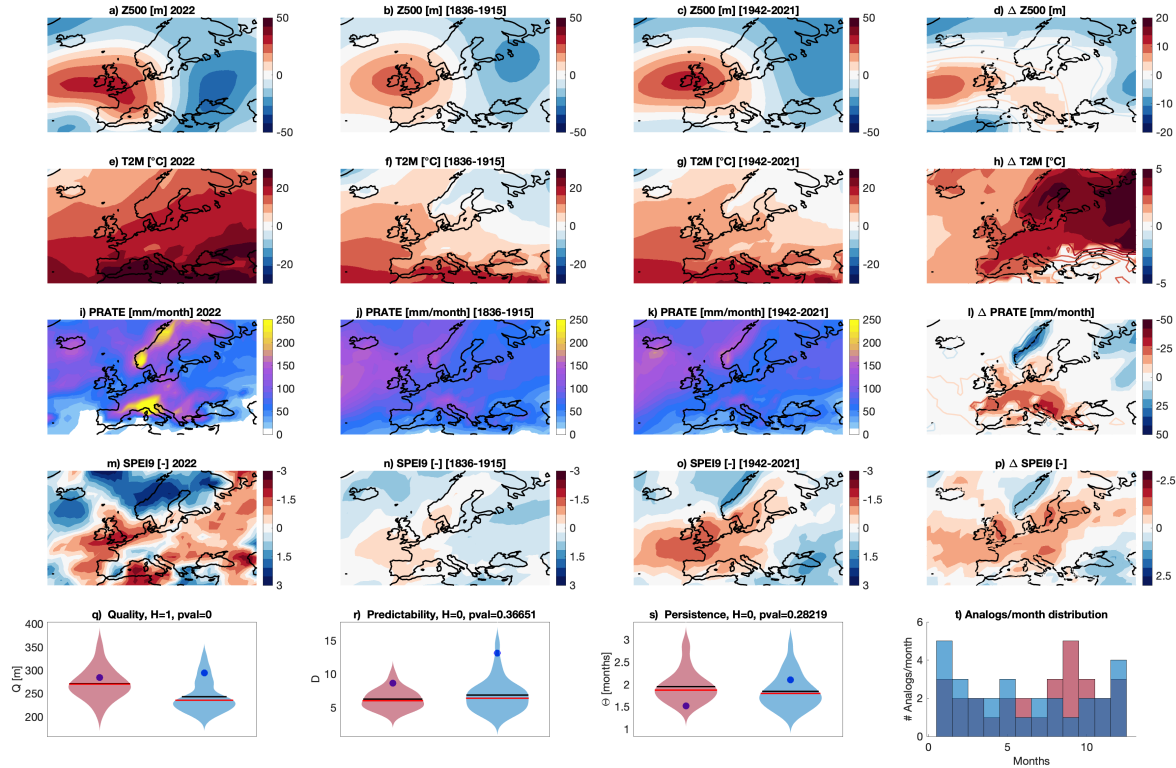


Figure 2. Attribution results for the 2022 Drought via analogs. December 2021 to August 2022 averaged mean 500 hPa geopotential height field Z500 (a), 2-meter temperatures T2M (e), monthly precipitation rate PRATE (i), SPEI9 index (m). Average of the 29 Z500 analogs found for the counterfactual [1836-1915] (b) and factual [1941-2021] (c) periods and corresponding 2-meter temperatures (f,g), daily precipitation rate (j,k) and SPEI9 (n,o). $\Delta Z500$ (d), $\Delta T2M$ (h), $\Delta PRATE$ (i) and $\Delta SPEI9$ (p) between factual and counterfactual periods: colored-filled areas show significant anomalies with respect to the bootstrap procedure. Violin plots for counterfactual (blue) and factual (orange) periods for the analogs Quality Q (q) the Predictability index D (r), the Persistence index Θ (s) and the distribution of analogs in each month (t). Black (red) lines in violin plots indicate mean (median) values. Titles in violin plots report the results H of the two-sided Cramér-von Mises test at the 0.05 significance level with the corresponding p-values (see section 2.4 for details).

267 The predictability (Fig. 2r) and the persistence (Fig. 2s) of the analogs do not show
 268 significant differences between the counterfactual and factual climates. The seasonality
 269 of the analogs (Fig. 2t) shows a tendency of observing such Z500 anomalies more in
 270 the summer and early autumn months in the factual period than in the counterfactual
 271 period. Supplementary Fig. S4-S10 show that this analysis is overall fairly qualitative
 272 insensitive to the choice of the variable (Z500 or SLP) or the dataset or the bias-
 273 correction procedure employed, with the exception of the persistence of the analogs,
 274 which show a tendency to be more common in winter and spring in the factual climate
 275 when SLP is employed.

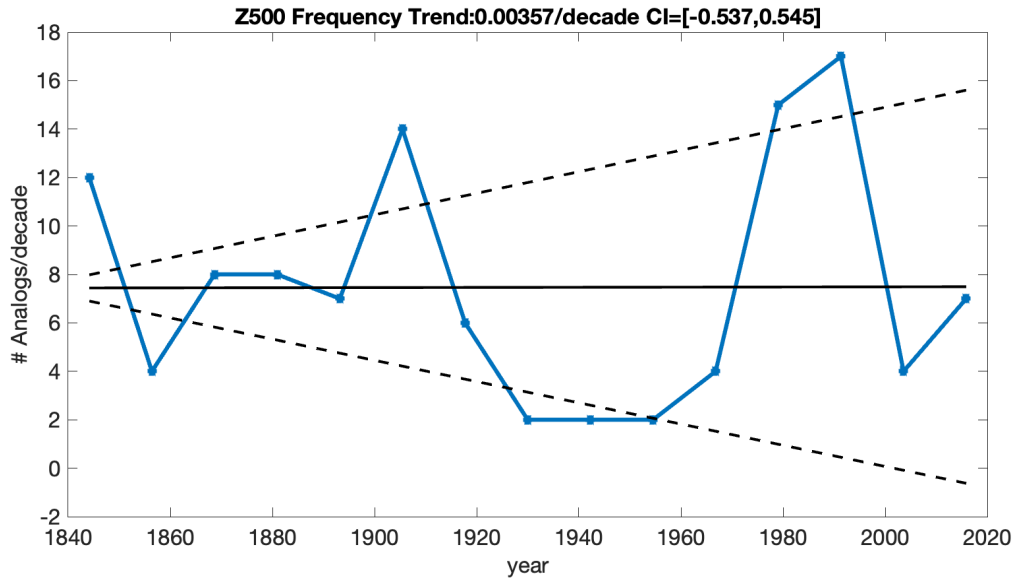


Figure 3. Evolution of the Frequency of analogs per decade. Evolution of the number of analogs per decade. In this case, analogs are computed for all the period 1836-2021. A linear fit is performed and the 95% confidence intervals (CI) of the a parameter of the fit using the Wald method [42]

276 3.3. Frequency of occurrence

277 In order to determine whether the atmospheric circulation that led to the 2022 drought
 278 (Fig. 1a, Fig. 2a) has become more frequent in the factual climate, we now examine
 279 whether there is a trend in the frequency of the associated analogs over the whole 1836-
 280 2021 period, again leaving the year 2022 outside of this search. For this analysis, we
 281 set the quantile for the analogs search to 0.95, i.e. we consider the 5% closest analogs
 282 to the event, to have enough analogs in each decade to estimate a robust trend. We
 283 have however tested trends obtained for higher quantiles (0.97, 0.98), i.e. looking at the
 284 3% and 2% closest analogs without finding qualitative differences. Results are shown
 285 in Figure 3, where we can see the number of analogs per decade. We estimate a linear
 286 trend $ax + b$ where x is the number of analogs per decade and the upper and lower
 287 95% confidence intervals (CI) of the a parameter of the fit using the Wald method [42].
 288 The analysis shows an increasing variability in the frequency of the analogs without
 289 any significant increasing or decreasing trends. Similar results are obtained for SLP
 290 and other datasets (Fig. S11-S17). This leads us to conclude that the slow-evolving
 291 component of the circulation anomaly that drove the 2022 drought has not become
 292 more frequent in recent decades.

293 3.4. Dependence on ENSO and AMO

294 Finally, we examine the association of the analogs with two major modes of interannual
 295 and interdecadal variability, namely ENSO and AMO. We build the probability

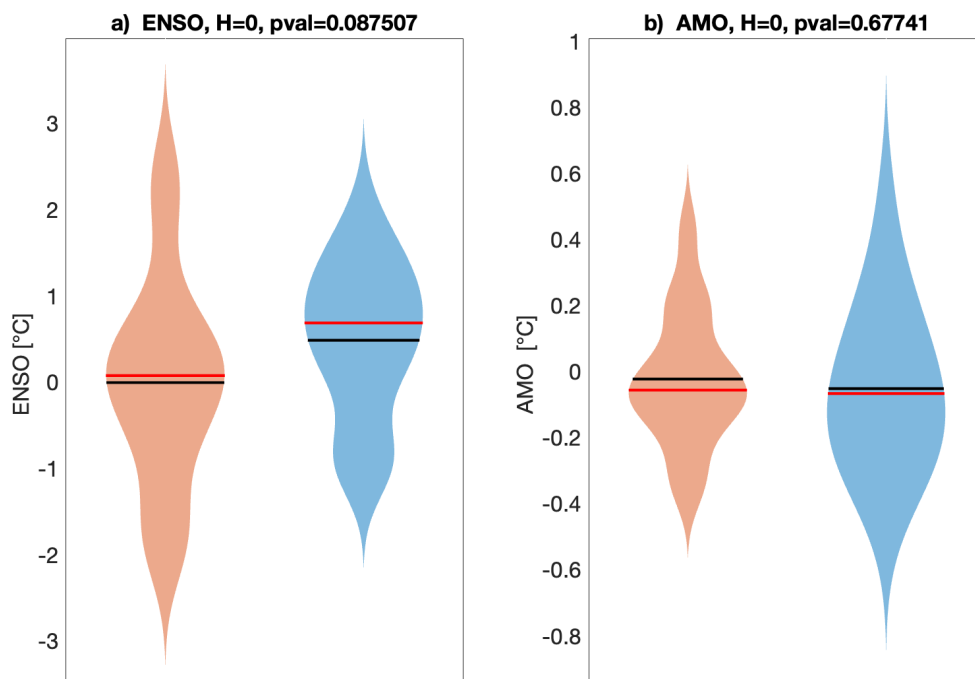


Figure 4. Analysis of the interannual and interdecadal variability. Violin plots for counterfactual (blue) and factual (orange) periods for ENSO (a) and AMO (b) values corresponding to the analogs months. Titles in violin plots report the results H of the two-sided Cramér-von Mises test at the 0.05 significance level with the corresponding p-values (see section 2.4 for details).

296 distributions of the values of the ENSO and AMO indices selected at the months of
 297 the occurrence of analogs. If there exists a strong association between ENSO or AMO,
 298 and the circulation anomaly of Fig. 2a, then we would find a probability distribution
 299 not centered around zero.

300 The results are shown in Fig. 4a for ENSO and in Fig. 4b for AMO. For the
 301 dataset used in the main text (20CRv3 plus NCEP/DOE) the analysis shows: (1) no
 302 significant changes in the distribution of ENSO (AMO) between the counterfactual and
 303 factual world, and (2) no tendency for El Niño or La Niña (positive AMO or negative
 304 AMO) to prevail during periods characterized by circulation analogs of the one seen
 305 during December 2021-August 2022. That would seem to reinforce our initial conjecture
 306 (Sect. 1) of no strong association between La Niña and the 2022 drought.

307 We note however that the p-value of the test for ENSO is equal to 0.088, close
 308 to the significance value of 0.05. Indeed some of the supplementary datasets shown
 309 in Fig. S18, S20, S21 show a significant change in the distribution of ENSO between
 310 the counterfactual and factual climate. Hence, we cannot completely reject a moderate
 311 role of interannual variability in exacerbating the 2022 drought. Interestingly, the same
 312 analysis performed for the sea-level pressure patterns (Figs. S22-S24) show instead a

313 dependence on the AMO but not on the ENSO.

314 4. Discussion

315 We find a prominent role of the atmospheric circulation in driving the 2022 drought.
316 There is a strong correspondence between the areas where Z500 was higher in the 2022
317 and the anomaly of this quantity in the factual vs counterfactual period. In particular,
318 the geopotential height is not just higher but the area with positive anomalies is also
319 larger. As a consequence, while in the counterfactual periods droughts associated with
320 these synoptic situations were confined to the British Isles, France, and partially the
321 Iberian peninsula, in the factual world they embrace a larger portion of continental
322 Europe and Italy. There is therefore a sort of “inflating balloon” effect which expands the
323 spatial extent of the drought and makes the anticyclonic dome higher, thus contributing
324 to increasing the severity of the 2022 drought. This is a “thermodynamic” effect of global
325 warming [43]. In addition to that, we also found that factual analogs get “warmer”, i.e.,
326 the near-surface temperature associated with them becomes higher (Fig. 2h). That leads
327 to a more negative value of SPEI even if PRATE remains unchanged because higher
328 surface temperature increases evapotranspiration, which dries the soil. This result is in
329 line with [3], which focused on the on exceptionality of the June-August soil moisture
330 deficit in Europe and found that human-induced climate change made the 2022 root
331 zone soil moisture drought about 3-4 times more likely, and the surface soil moisture
332 drought about 5-6 times more likely.

333 While the “balloon” expansion effect of Z500 is the most visible, we also note a
334 change in the shape of the anticyclonic structure going from the counterfactual and
335 factual periods, with the positive Z500 anomaly featuring a “crescent” shape from the
336 Atlantic through Central Europe into the Mediterranean (Fig. 2d). While this change in
337 shape is of dynamical nature and thus related to systematic changes in the atmospheric
338 circulation goes beyond the scope of this study, but would deserve further attention in
339 future studies.

340 No trends in the frequency of this pattern have been observed but an increase in the
341 interdecadal variability of occurrence which becomes larger recently with decades where
342 this pattern is basically absent and decades where it is more frequent. This looks in
343 line with the IPCC statements on the increase of variability of our climate under ACC
344 [41]. Finally, the analysis of the interannual and interdecadal oceanic variability on the
345 2022 drought suggests that we cannot completely rule out the influence of ENSO for the
346 upper-level circulation and for the Atlantic Multi-decadal Oscillation for the lower-level
347 circulation, although such influences are likely to be very modest.

348 5. Conclusions

349 According to the World Meteorological Organization, drought represents one of the most
350 damaging and life-threatening climate-related hazards [44]. The attribution of drought

351 events to human-caused climate change is not as clear as for other types of weather
352 hazards like, e.g., heatwaves, because of the confounding role of natural variability
353 [18]. Exceptional droughts have in fact occurred over the last two thousand years in
354 association with decadal variations in sea surface temperatures [45]. While the last
355 IPCC 6th Assessment Report states that we have “medium confidence” in attributing
356 to human-induced climate change the increases in agricultural and ecological droughts
357 because of increased land evapotranspiration [46, 41, 47], attribution to human-caused
358 climate change of meteorological droughts – directly related to rainfall deficits and hence
359 to atmospheric dynamics – remains challenging. Nevertheless, progress has been made
360 and recent research highlighted the role of global warming in the exacerbation of some
361 recent extraordinary meteorological droughts [48, 49, 19, 20].

362 In this study we considered the 2022 European-Mediterranean drought [1, 2]
363 and investigated the exceptionality of the event and of its atmospheric drivers in a
364 century-long reanalysis (1836-2021) using the analog-based methodology proposed in
365 [17]. Our results indicate a role for ACC in making the atmospheric anticyclonic
366 anomaly “stronger” and “warmer”, two facts that in turn caused more widespread and
367 exacerbated drought conditions. Conversely, we found that the frequency of occurrence
368 of such a slow-evolving circulation component has not significantly changed over the
369 last two centuries. These conclusions highlight a thermodynamic component in the
370 exacerbation of droughts by human-caused global warming, while no strong evidence
371 was found about a dynamical component - i.e., a change in circulation – in the recent
372 period which could have triggered the 2022 drought.

373 While our study heavily relies on the observational datasets used and does not
374 employ climate models, our results appear robust to the choice of meteorological
375 variables and reanalysis. They further illustrate the capability of a reanalysis-based
376 attribution conditioned on the atmospheric circulation on longer time-scales suggesting
377 that this methodology could also be used to investigate other long-lasting events driven
378 by synoptic situations such as prolonged cold periods or heatwaves.

379 An approach based only on observations, like the one applied in this study, while
380 providing important information on the likelihood of the 2022 drought, has some
381 limitations for attributing this extreme event to human-caused climate change, that
382 is, first, the impossibility to define a counterfactual climate with no anthropogenic
383 forcing and, second, the limited number of years available in reanalyses datasets. In
384 a follow-up study thus we plan to complement this study by applying this method to
385 climate models too, and in particular to single model initial-condition large ensembles
386 [50, 51, 52, 19, 53]. While these models are affected by systematic biases which can
387 compromise their realism, they allow for a more rigorous definition of factual and
388 counterfactual climate, and provide thousands of years of data is available for more
389 robust statistics.

390 Acknowledgments

391 D. F. received support from the European Union's Horizon 2020 research and innovation
392 programme under grant agreement No. 101003469 (XAIDA) and the Marie Skłodowska-
393 Curie grant agreement No. 956396 (EDIPI).

394

395 Author Contributions

396 S.P. devised the study, D.F. performed the analyses and B.B. prepared the datasets and
397 performed the bias corrections. All authors contributed to discussing and writing the
398 paper.

399 Competing Interest

400 The authors declare no competing interests nor conflicts of interest. No human or animal
401 data have been used in this study.

402 Data Availability

403 The data that support the findings of this study are available upon request from the
404 authors. In addition, all other input data (SLP, Z500, T2M, and PRATE), climate
405 indices (ENSO and AMO), and observed drought index (SPEI9) used in this study are
406 publicly available at <https://psl.noaa.gov/data/gridded/>, <https://climexp.knmi.nl>, and
407 <https://spei.csic.es/map/>, respectively.

408 References

- 409 [1] Toreti A, Bavera D, Avanzi F, Cammalleri C, De Felice M, de Jager A, Di Ciollo C, Gabellani
410 S, Maetens W, Magni D, Manfron G, Masante D, Mazzeschi M, McCormick N, Naumann G,
411 Niemeyer S, Rossi L, Seguini L, Spinoni J and van den Berg M 2022 JRC128974
- 412 [2] Toreti A, Bavera D, Acosta Navarro J, Cammalleri C, de Jager A, Di Ciollo C, Hrast Essenfelder
413 A, Maetens W, Magni D, Masante D, Mazzeschi M, Niemeyer S and Spinoni J 2022 *Publications*
414 *Office of the European Union, Luxembourg* JRC130493
- 415 [3] Schumacher D L, Zachariah M, Otto F, Barnes C, Philip S, Kew S, Vahlberg M, Singh R, Heinrich
416 D, Arrighi J, van Aalst M, Thalheimer L, Raju1 E, Hauser M, Hirschi M, Gudmundsson L,
417 Beaudoin H K, Rodell M, Li S, Yang W, Vecchi G A, Vautard R, Harrington L J and Seneviratne
418 S I 2022 *WWA: World Weather Attribution*
- 419 [4] Vicente-Serrano S, Beguería S and I L J 2010 *J. Climate* **23** 1696–1718
- 420 [5] Baruth B, Bassu S, W B, Biavetti I, Bratu M, Cerrani I, Chemin Y, Claverie M, De Palma P,
421 Fumagalli D, Manfron G, Morel J, Nisini L, Panarello L, Ronchetti G, Seguini L, Tarnavsky
422 E, van den Berg M, Zajac Z and Zucchini A 2022 *JRC MARS Bulletin* **30** URL <https://ec.europa.eu/jrc/en/mars/bulletins>
- 423
- 424 [6] Mishra A K and Singh V P 2010 *J. Hydrol.* **391** 202–216

- 425 [7] Afshar M, Bulut B, Duzenli E, Amjad M and Yilmaz M 2022 *Agricultural and Forest Meteorology*
426 **316** 108848
- 427 [8] Miralles D, Gentile P, Seneviratne S I and Teuling A J 2019 *Ann. N. Y. Acad. Sci.* **1436** 19–35
- 428 [9] Brönnimann S, Xoplaki E, Casty C, Pauling A and Luterbacher J 2007 *Clim. Dyn.* **28** 181–197
- 429 [10] Brönnimann S 2007 *Rev. Geophys.* **45** RG3003
- 430 [11] López-Parages J, Rodríguez-Fonseca B, Dommenges D and Frauen C 2016 *Clim. Dynamics* **47**
431 2071–2084
- 432 [12] Reuters 2022
- 433 [13] Bost A F, Villeneuve A, Armand M, Zabalza F, Gauchard Y, Foucart S and Rof G 2022 *Le Monde*
- 434 [14] Kaleem J and Johnson S 2022 *Los Angeles Times*
- 435 [15] Yiou P, Jézéquel A, Naveau P, Otto F E L, Vautard R and Vrac M 2017 *Adv. Stat. Clim. Meteorol.*
436 *Oceanogr.* **3** 17–31
- 437 [16] Otto F E L 2017 *Annu. Rev. Environ. Resour.* **42** 627–646
- 438 [17] Faranda D, Bourdin S, Ginesta M, Krouma M, Noyelle R, Pons F, Yiou P and Messori G 2022
439 *Weather Clim. Dynam.* **3** 1311–1340
- 440 [18] NAS 2016 *Natl. Acad. Sci. Eng. Med.* 166pp
- 441 [19] Pascale S, Kapnick S and Delworth T Land Cooke W 2020 *Proceedings of the National Academy*
442 *of Sciences of the United States of America* **117** 29495–29503
- 443 [20] Pascale S, Kapnick S, Delworth T, Hidalgo H and Cooke W 2021 *Climatic Change* **168** 1–21
- 444 [21] van der Wiel K, Lenderink G and de Vries H 2021 *Weather and Climate Extremes* **33** 100350
445 ISBN: 2212-0947 Publisher: Elsevier
- 446 [22] Beguería S, Vicente-Serrano S, Reig F and Latorre B 2014 *Int. J. Climatol.* **34** 3001–3023
- 447 [23] Hayes M, Wilhite D, Svoboda M and Vanyarkho 1999 *Bulletin of the American Meteorological*
448 *Society* **80** 429–438
- 449 [24] Adams H, Guardiola-Claramonte M, Barron-Gafford G A, Villegas J C, Breshears D D, Zou C B,
450 Troch P A and Huxman T E 2009 *Proceedings of the National Academy of Sciences of the United*
451 *States of America* **106** 7063–7066
- 452 [25] Slivinski L C, Gilbert P C, Jeffrey S W, Sardeshmukh P D, Giese B S, McColl C, Allan R, Yin X,
453 Vose R, Titchner H, Kennedy J, Spencer L J, Ashcroft L, Brönnimann S, Brunet M, Camuffo D,
454 Cornes R, Cram T A, Crouthamel R, Domínguez-Castro F, Freeman J E, Gergis J, Hawkins E,
455 Jones P D, Jourdain S, Kaplan A, Kubota H, F L, Lee T C, Lorrey A, Luterbacher J, Maugeri
456 M, Mock C J, Kent Moore G, Przybylak R, Pudmenzky C, Reason C, Slonosky V C, Smith
457 C A, Tinz B, Trewin B, Valente M A, Wang X L, Wilkinson C, Wood K and Wyszynski P 2019
458 *Q. J. R. Meteorol. Soc.* **724** 2876–2908
- 459 [26] Kalnay E, Kanamitsu M, Kistler R, Collins W, Deaven D, Gandin L, Iredell M, Saha S,
460 White G, Woollen J, Zhu Y, Chelliah M, Ebisuzaki W, Higgins W, Janowiak J, Mo K C,
461 Ropelewski C, Wang J, Leetmaa A, Reynolds R, Jenne R and Joseph D 1996 *Bulletin of the*
462 *American Meteorological Society* **77** 437–472 ISSN 0003-0007 URL [https://doi.org/10.1175/
463 1520-0477\(1996\)077<0437:TNYRP>2.0.CO;2](https://doi.org/10.1175/1520-0477(1996)077<0437:TNYRP>2.0.CO;2)
- 464 [27] Huang B, Thorne P W, Banzon V F, Boyer T, Chepurin G, Lawrimore J H, Menne M J, Smith
465 T M, Vose R S and Zhang H M 2017 *Journal of Climate* **30** 8179–8205
- 466 [28] Trenberth K E and Shea D J 2006 *Geophysical research letters* **33**
- 467 [29] Freitas A C M, Freitas J M and Todd M 2011 *Journal of Statistical Physics* **142** 108–126
- 468 [30] Freitas A C M, Freitas J M and Vaienti S 2016 *arXiv preprint arXiv:1605.06287*
- 469 [31] Lucarini V, Faranda D, Freitas A C M, Freitas J M, Holland M, Kuna T, Nicol M, Todd M
470 and Vaienti S 2016 *Extremes and recurrence in dynamical systems* (John Wiley & Sons) ISBN
471 1-118-63219-2
- 472 [32] Faranda D, Messori G and Yiou P 2017 *Scientific reports* **7** 41278 URL [https://www.nature.
473 com/articles/srep41278.pdf](https://www.nature.com/articles/srep41278.pdf)
- 474 [33] Faranda D, Messori G and Vannitsem S 2019 *Tellus A: Dynamic Meteorology and Oceanography*
475 **71** 1–11

- 476 [34] Faranda D, Messori G and Yiou P 2017 *Scientific reports* **7** 41278
- 477 [35] Messori G, Caballero R and Faranda D 2017 *Geophysical Research Letters* **44** 3346–3354
- 478 [36] Hochman A, Alpert P, Harpaz T, Saaroni H and Messori G 2019 *Science advances* **5** eaau0936
- 479 [37] Faranda D, Vrac M, Yiou P, Jézéquel A and Thao S 2020 *Geophysical Research Letters* **47**
480 e2020GL088002
- 481 [38] Trenberth K E 2011 *Wiley Interdisciplinary Reviews: Climate Change* **2** 925–930
- 482 [39] Anderson T W 1962 *The Annals of Mathematical Statistics* 1148–1159
- 483 [40] Dorrington J, Strommen K and Fabiano F 2022 *Weather and Climate Dynamics* **3** 505–533
- 484 [41] Allan R P, Hawkins E, Bellouin N and Collins B 2021
- 485 [42] Stein C and Wald A 1947 *The Annals of Mathematical Statistics* 427–433
- 486 [43] Faranda D, Vrac M, Yiou P, Jézéquel A and Thao S 2020 *Geophys. Res. Lett.* **47** e2020GL088002
487 iSBN: 0094-8276 Publisher: Wiley Online Library
- 488 [44] World Meteorological Organization 2021 Weather-related disasters in-
489 crease over past 50 years, causing more damage but fewer
490 deaths URL [https://public.wmo.int/en/media/press-release/
491 weather-related-disasters-increase-over-past-50-years-causing-more-damage-fewer](https://public.wmo.int/en/media/press-release/weather-related-disasters-increase-over-past-50-years-causing-more-damage-fewer)
- 492 [45] Cook B I, Smerdon J E, Cook E R, Park Williams A, Anchukaitis K J, Mankin J S, Allen K,
493 Andreu-Hayles L, Ault T R, Belmecheri S, Coats S, Coulthard B, Fosu B, Grierson P, Griffin
494 D, Herrera D A, a Ionita M, Lehner F, Leland C, Marvel K, Morales M S, Mishra V, Ngoma J,
495 Nguyen H T T, O’Donnell A, Palmer J, Rao M P, Rodriguez-Caton M, Seager R, Stahle D W,
496 Stevenson S, Thapa U K, Varuolo-Clarke A M and Wise E K 2022 *Nat. Rev. Earth Environ.* **3**
497 741–757
- 498 [46] Herrera D A, Ault T R, Fasullo J T, Coats S J, Carrillo C M, Cook B I and Williams A P 2018
499 *Geophysical Research Letters* **45** 10,619–10,626
- 500 [47] Seneviratne S, Zhang X, Adnan M, Badi W, Dereczynski C, Luca A D, Ghosh S, Iskandar I, Kossin
501 J, Lewis S, Otto F, Pinto I, Satoh M, Vicente-Serrano S, Wehner M, and Zhou B 2021
- 502 [48] Fischer E M, Seneviratne S I, Lüthi D and Schär C 2007 *Geophysical Research Letters* **34**
- 503 [49] Otto F E L, Wolski P, Lehner F, Tebaldi C, van Oldenborgh G, Hogesteeger S, Singh R, Holden
504 P, Fuckar N, Odoulami R and New M 2018 *Environ. Res. Lett.* **13** 124010
- 505 [50] Lehner F, Coats S, Stocker T F, Pendergrass A G, Sanderson B M, Raible C C, and Smerdon J E
506 2017 *Geophys. Res. Lett.* **44** 7419–7428
- 507 [51] Deser C, Lehner F, Rodgers K B, Ault T, Delworth T L, DiNezio P N, Fiore A, Frankignoul C,
508 Fyfe J C and Horton D E 2020 *Nature Climate Change* 1–10 iSBN: 1758-6798 Publisher: Nature
509 Publishing Group
- 510 [52] Zscheischler J and Fischer E M 2020 *Weather and Climate Extremes* **29** 100270
- 511 [53] Gessner C, Fischer E M, Beyeler U and Knutti R 2022 *Weather and Climate Extremes* **38** 100512

Supplemental Material for “Persistent anticyclonic conditions and climate change exacerbated the exceptional 2022 European-Mediterranean drought”

Davide Faranda^{1,2,3}, Salvatore Pascale^{4,5}, Burak Bulut¹

¹ Laboratoire des Sciences du Climat et de l’Environnement, UMR 8212
CEA-CNRS-UVSQ, Université Paris-Saclay & IPSL, CE Saclay l’Orme des Merisiers,
91191, Gif-sur-Yvette, France

² London Mathematical Laboratory, 8 Margravine Gardens, London, W6 8RH,
British Islands

³ LMD-IPSL, Ecole Polytechnique, Institut Polytechnique de Paris, ENS, PSL
Research University, Sorbonne Université, CNRS, Palaiseau, France

⁴ University of Bologna, Department of Physics and Astronomy, Bologna, Italy

⁵ Centre for Sustainability and Climate Change, Bologna Business School, Bologna,
Italy

E-mail: davide.faranda@cea.fr, salvatore.pascale@unibo.it,
burak.bulut@cea.fr

Keywords: Drought - Climate Change - Attribution

1. Anomalies calculation for the analog analysis

In this section, we provided information about how anomalies of SLP and Z500 were calculated for the analog analysis.

Firstly, the normalization of the datasets is achieved in two steps; firstly, the raw data (x) is purged from its linear trend (x'), and secondly, the seasonality effect is removed by discarding long-time (1836-2022) monthly averages from corresponding months (x''). Secondly, the moving average of each month (x''') is obtained by taking the mean of the values from the related month and 8 months prior (i.e., for August, months between January and August). The results of each applied step to obtain anomalies are shown in (Fig [S2](#)).

2. Combining the 20CR and NCEP reanalyses and bias correction

In the following section, we describe why a bias correction is required before combining two reanalysis datasets and how we achieved the bias correction. In addition to the bias corrected datasets, we also provided merged datasets without using any correction.

It is required to merge two different datasets in order to provide uninterrupted data in the time period selected for the scope of the study. For this purpose, the 20CR dataset available between 01/1836 - 12/2015 and NCEP/DOE between 01/1979 - 08/2022 (and NCEP/NCAR 01/1948 - 08/2022) are combined. Firstly, all datasets are aggregated to the lowest resolution 2.5° using linear interpolation in order to eliminate the difference in spatial resolution. Then, it is necessary to eliminate the systematic difference between the two datasets, which has an effect on the calculation of the drought index. The linear rescaling method is used for the bias correction using the given equation below. The most linear relation between reference dataset X and the dataset to be rescaled Y is considered to implement the linear rescaling method in the form

$$Y^* = \mu_X + (Y - \mu_Y)c_Y \quad (1)$$

where Y^* is the rescaled version of Y, μ_X and μ_Y are time averages of X and Y, and c_Y is a scalar rescaling factor found by using variance-based linear methods as

$$c_Y = \sigma_X / \sigma_Y \quad (2)$$

where σ_X and σ_Y are standard deviations of X and Y datasets, respectively. Here in these equations, X and Y datasets refer to 20CR datasets and Reanalysis datasets within the commonly available period (01/1979 - 12/2015 for NCEP/DOE and 01/1948 - 12/2015 for NCEP/NCAR), respectively.

As a result, the datasets used in this study are obtained from the combination of all available raw 20CR datasets for the dates between 01/1836 - 12/2015, and either bias-corrected or not NCEP/DOE or NCEP/NCAR datasets for 01/2016 - 08/2022. The time series obtained with and without the bias correction method and the SPEI9 values, calculated from these two different time series are shown in (Fig. S3).

The Genova example showed that if we do not use bias correction when we merge two datasets and calculate SPEI9, it is not possible to catch drought events after 2016 due to the difference between the variables of the two datasets (Fig. S3 f). On the other hand, if we apply a linear rescaling method based on parameters obtained from the common years, we can calculate SPEI9 values (Fig. S3 g) consistent with the observed SPEI9 values obtained from SPEI Global Drought Monitor shown in the main text (Fig 1).

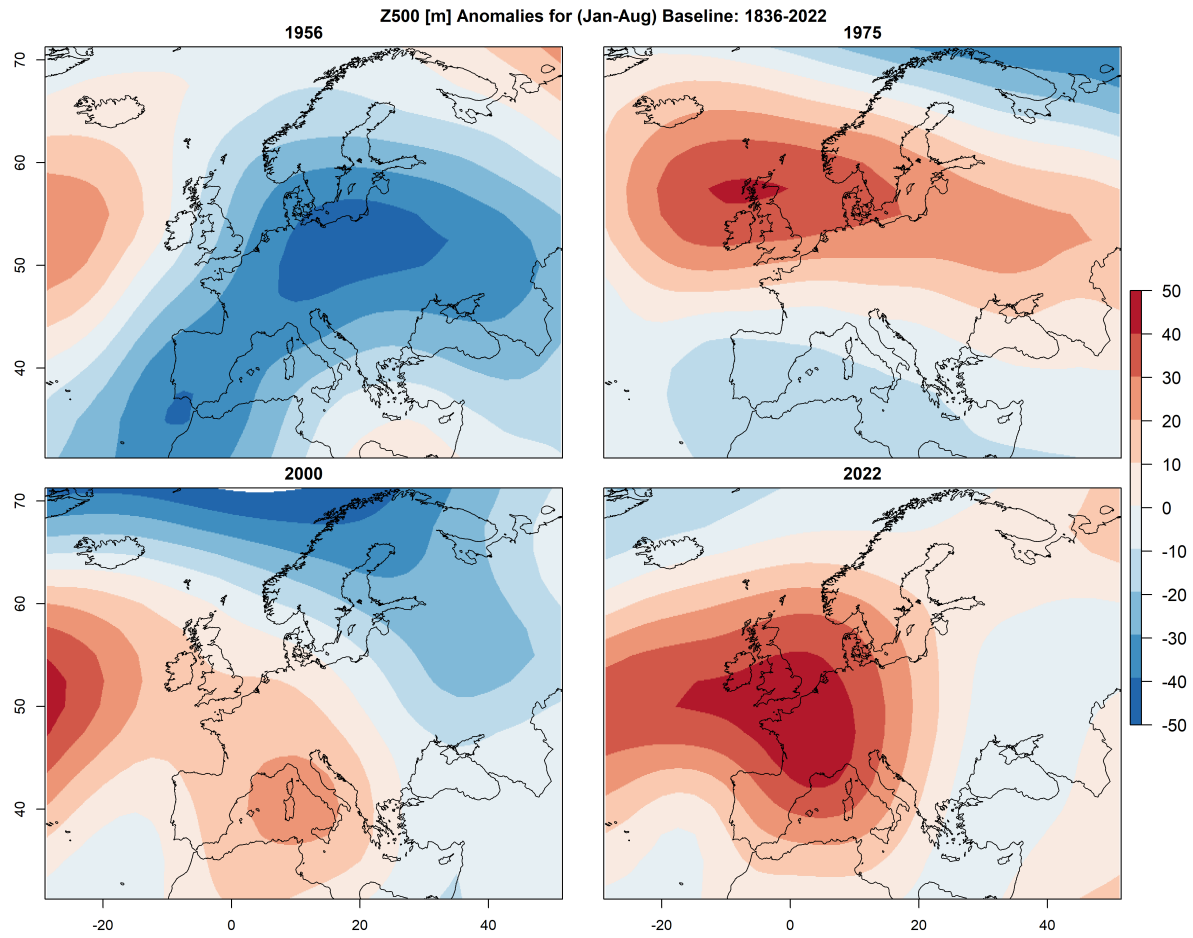


Figure S1. Circulation anomalies during persisting 3-year La Niña. 500 hPa January-to-August mean geopotential height anomaly in years (i.e., 1956, 1975, 2000, 2022) characterized by a three-year persisting La Niña.

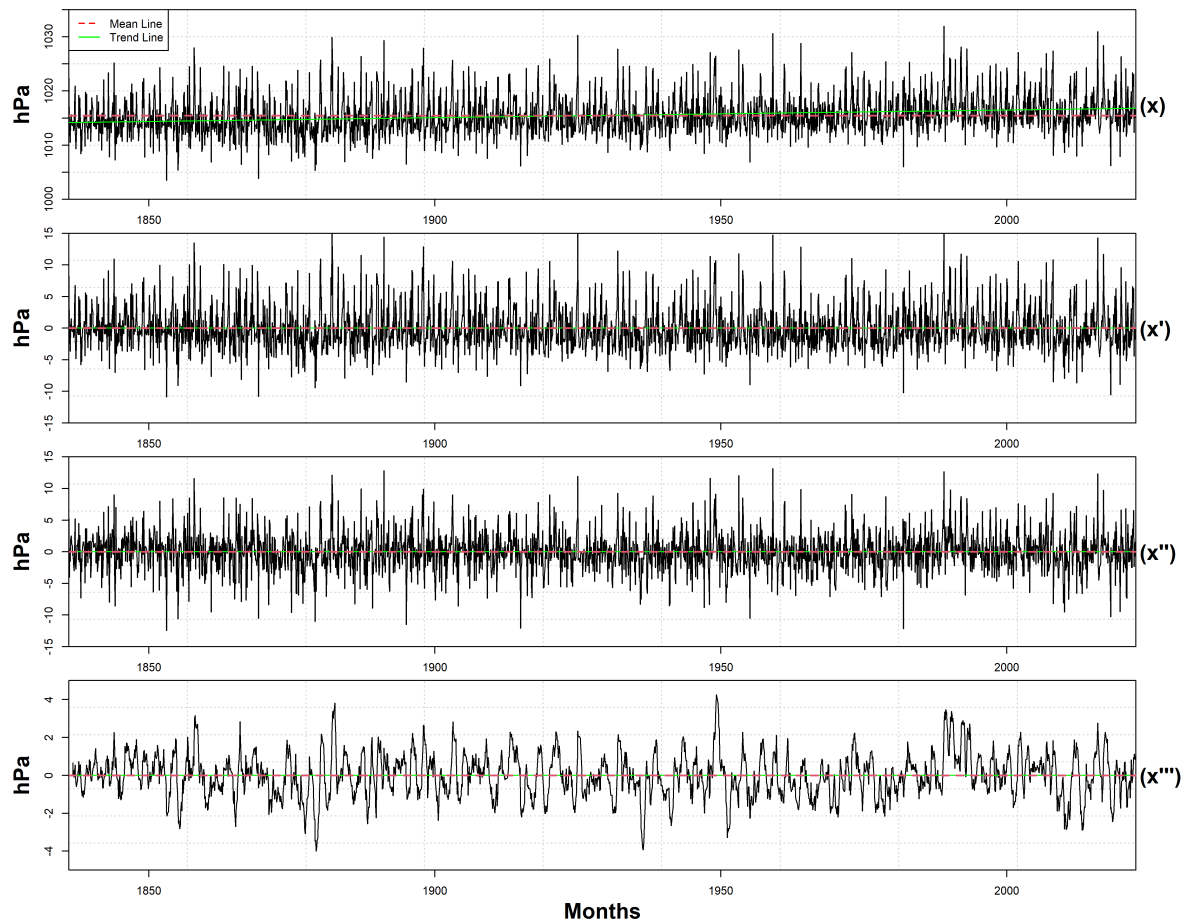


Figure S2. Example of the results at each step applied to obtain anomalies (SLP over Genova) time series of raw data (x), detrended data (x'), seasonality removed data (x''), and moving average applied data (x''').

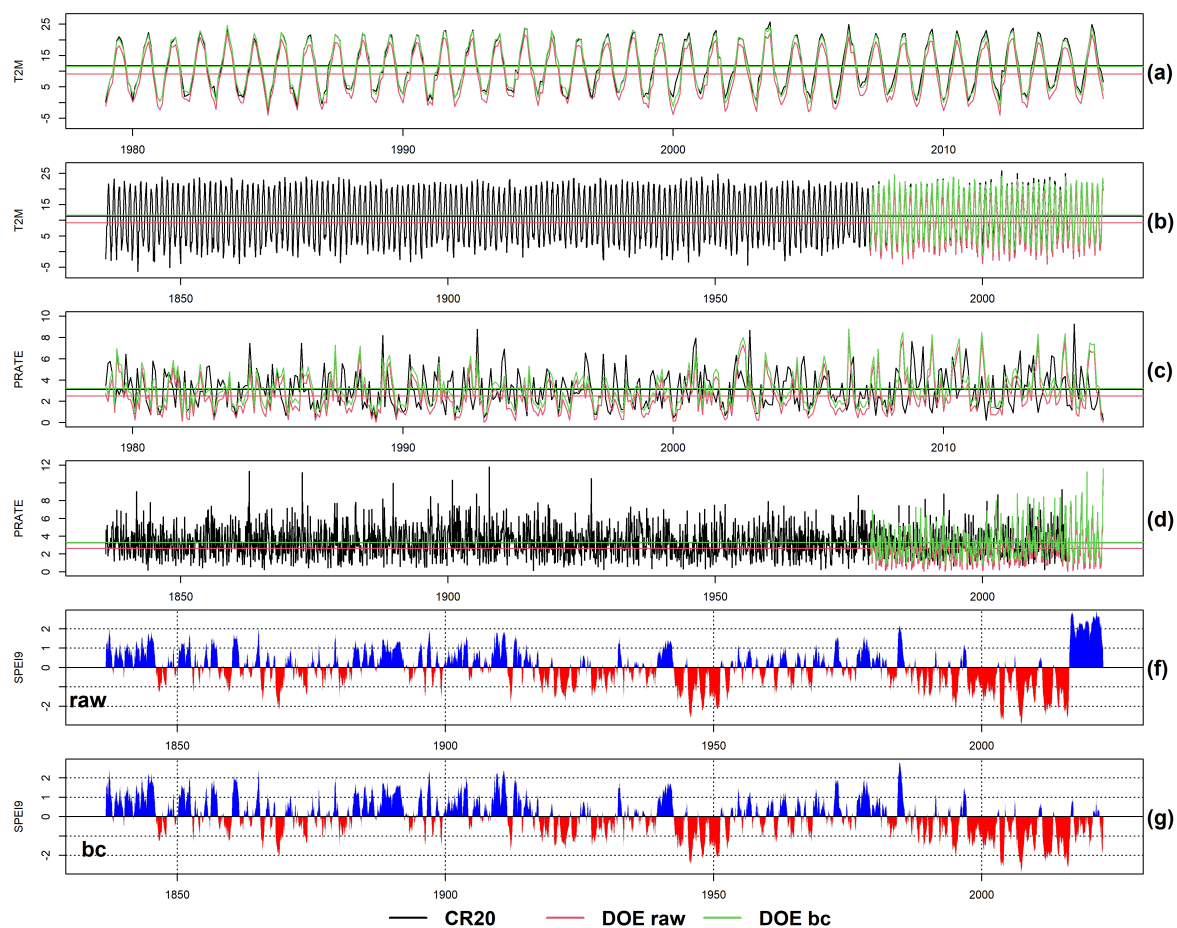


Figure S3. Comparisons of the time series obtained by combining 20CR and raw/bias-corrected NCEP/DOE T2M and PRATE time series for the common period (a,c) and complete study period (b,d), SPEI9 time series obtained from raw input datasets (e) and bias-corrected datasets (f) obtained over Genova. CR20, raw, and bias-corrected NCEP/DOE time series are shown in black, red, and green colors, respectively.

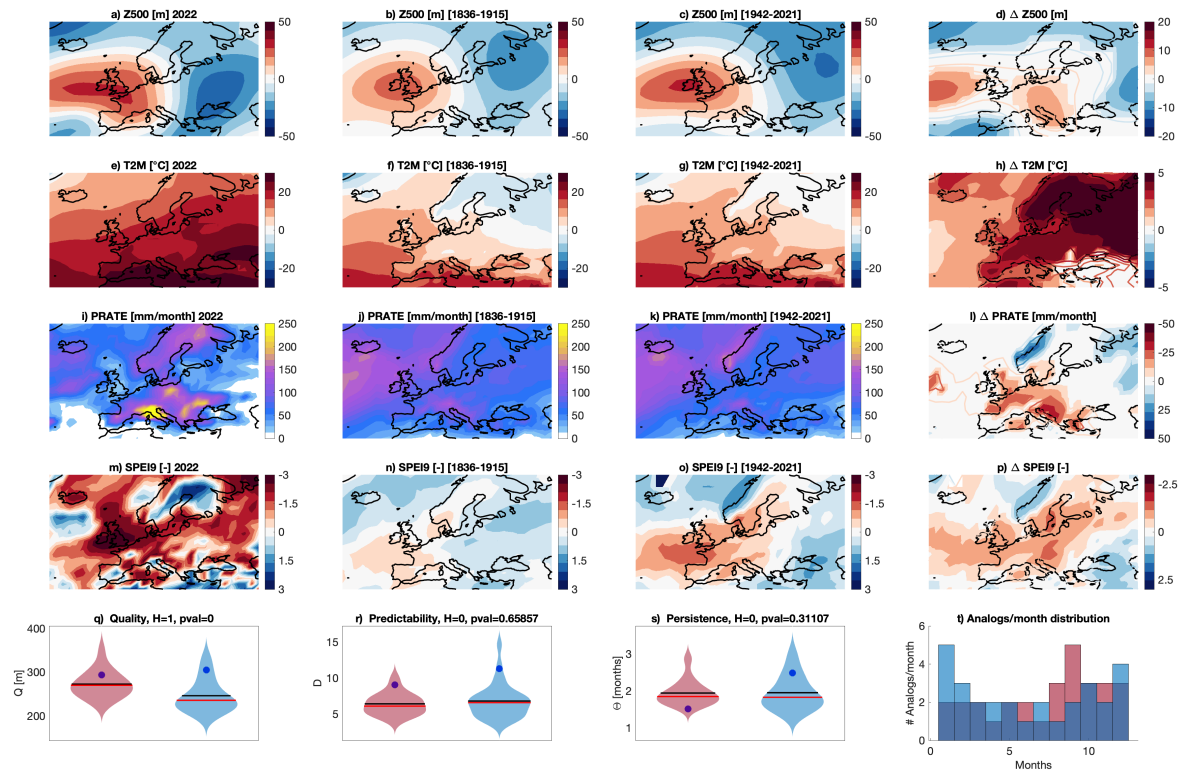


Figure S4. Attribution results for the 2022 Drought via analogs. As in Figure 2 in the main text, but for analogs of the non-bias corrected 500 geopotential height and the DOE dataset.

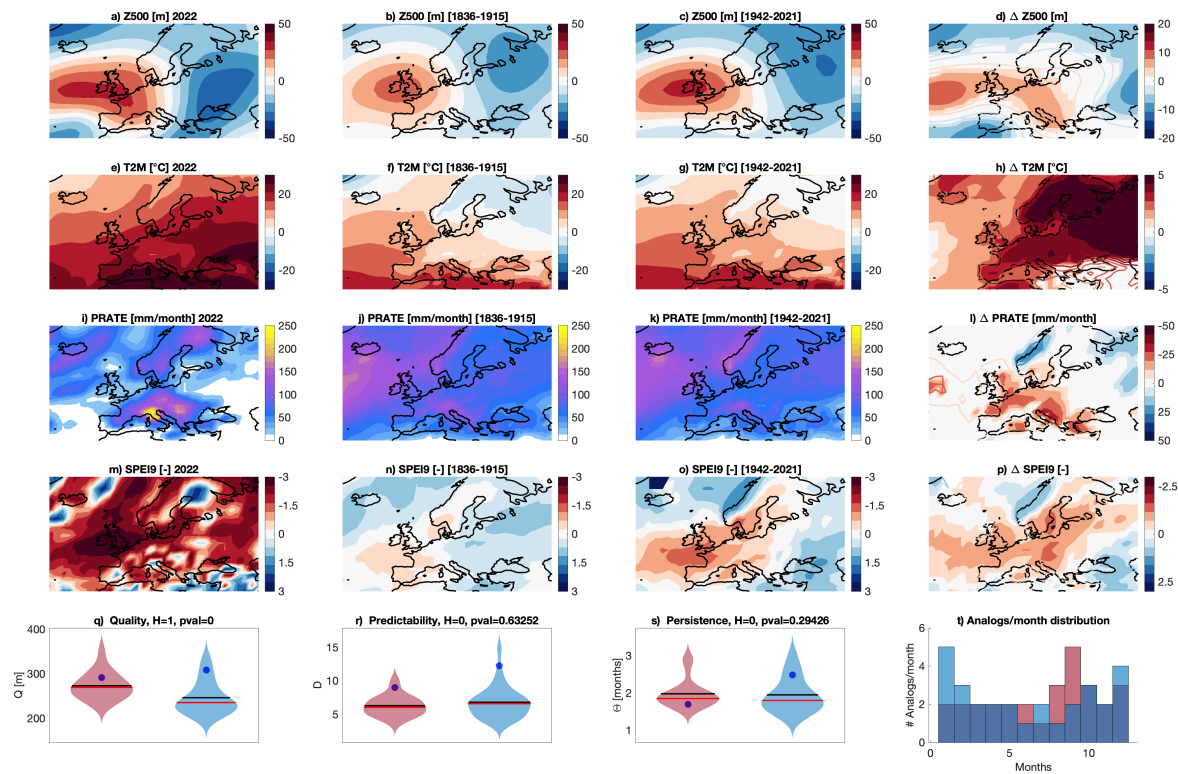


Figure S5. Attribution results for the 2022 Drought via analogs. As in Figure 2 in the main text, but for analogs of the non-bias corrected 500 geopotential height and the NCAR dataset.

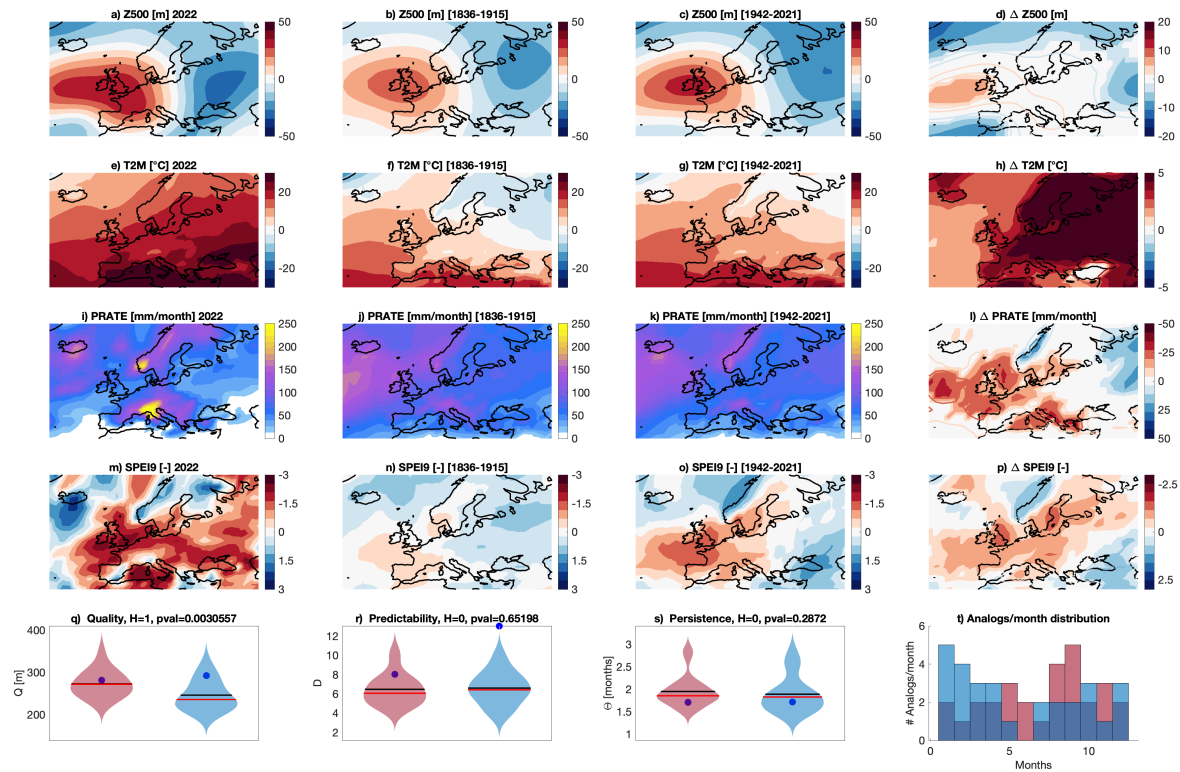


Figure S6. Attribution results for the 2022 Drought via analogs. As in Figure 2 in the main text, but for analogs of the bias corrected 500 geopotential height and the NCAR dataset.

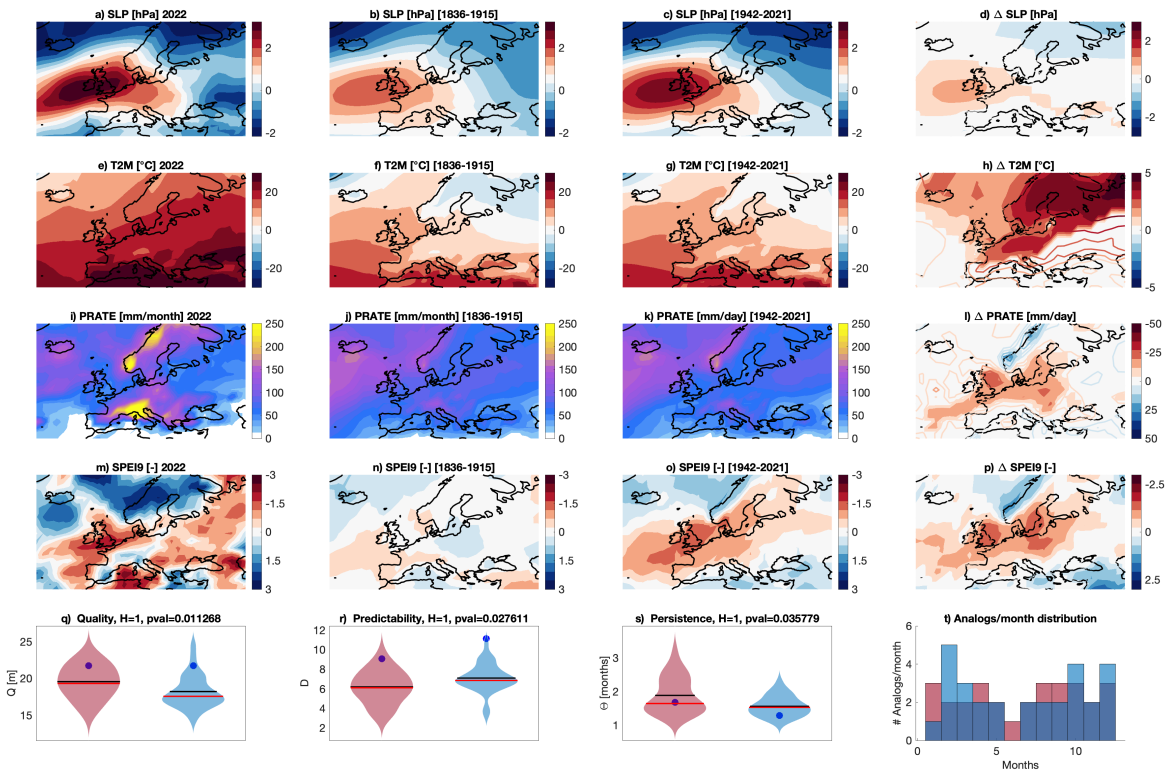


Figure S7. Attribution results for the 2022 Drought via analogs. As in Figure 2 in the main text, but for analogs of the bias corrected sea-level pressure and the DOE dataset.

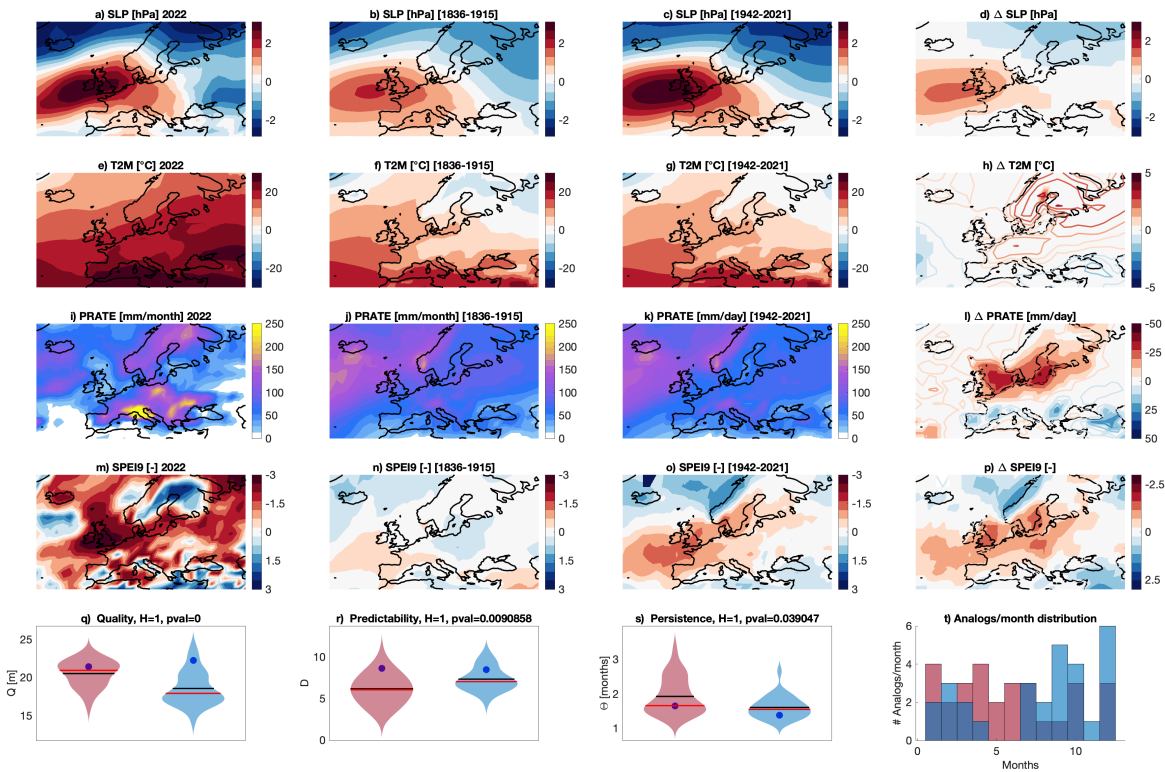


Figure S8. Attribution results for the 2022 Drought via analogs. As in Figure 2 in the main text, but for analogs of the non bias-corrected sea-level pressure and the DOE dataset.

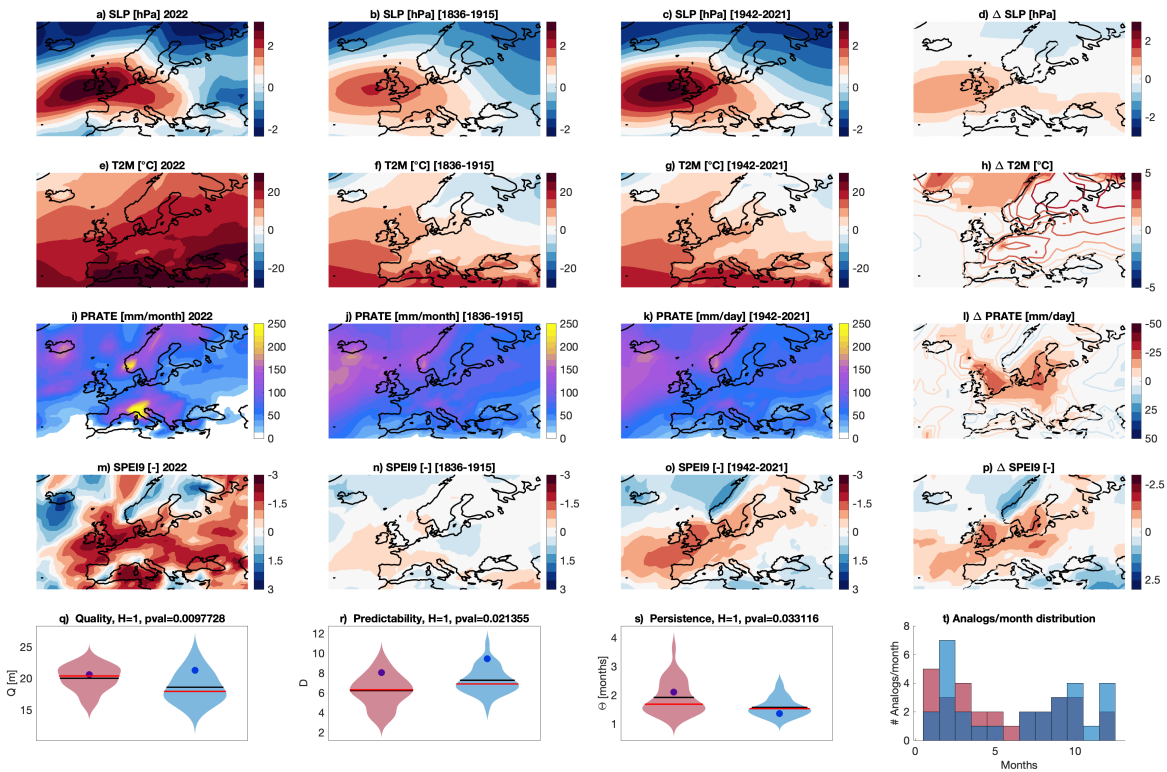


Figure S9. Attribution results for the 2022 Drought via analogs. As in Figure 2 in the main text, but for analogs of the bias corrected sea-level pressure and the NCAR dataset.

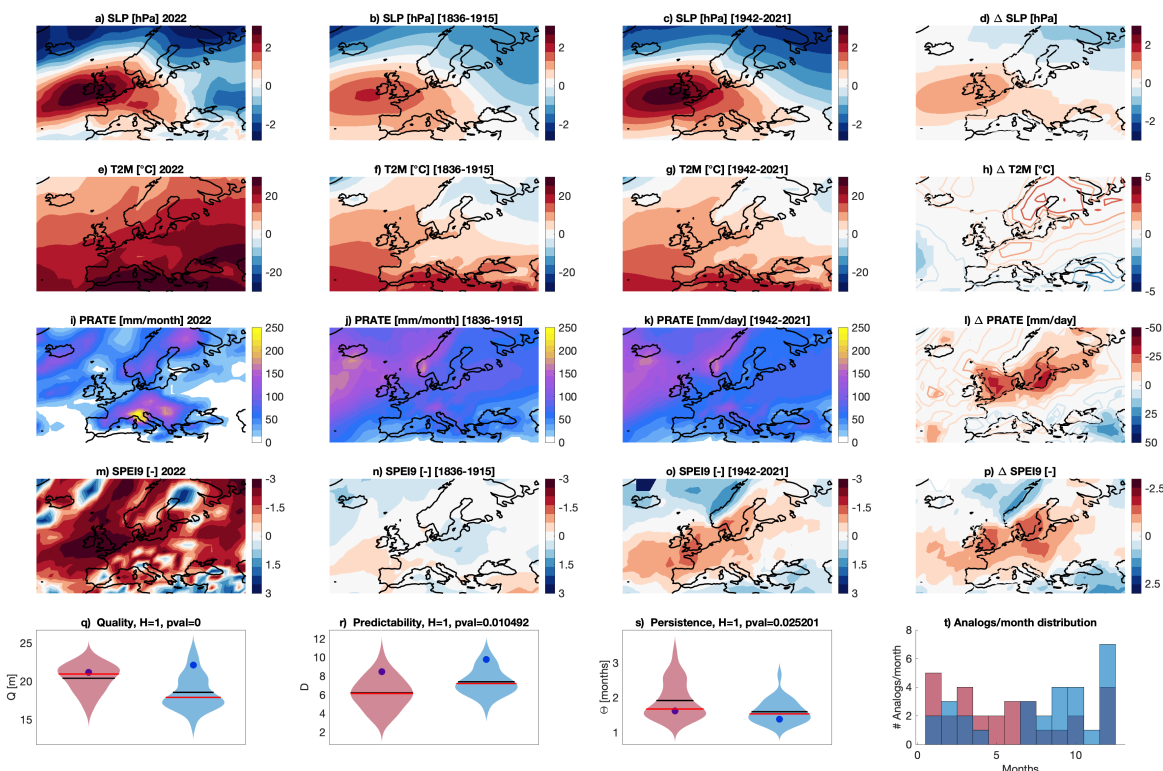


Figure S10. Attribution results for the 2022 Drought via analogs. As in Figure 2 in the main text, but for analogs of the non bias-corrected sea-level pressure and the NCAR dataset.

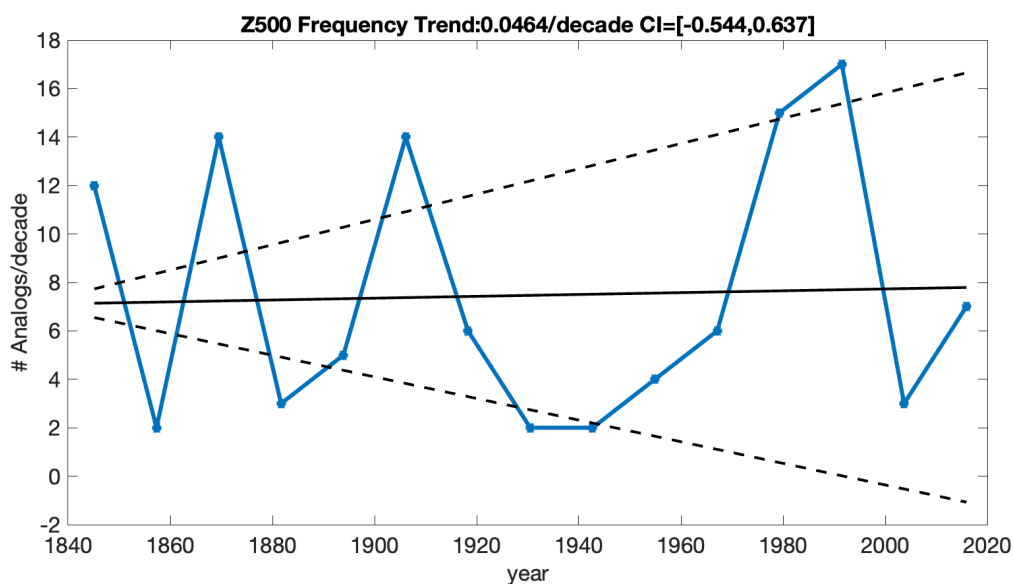


Figure S11. Evolution of the Frequency of analogs in time. As in Figure 3 in the main text, but for analogs of the non-bias corrected 500 geopotential height and the DOE dataset.

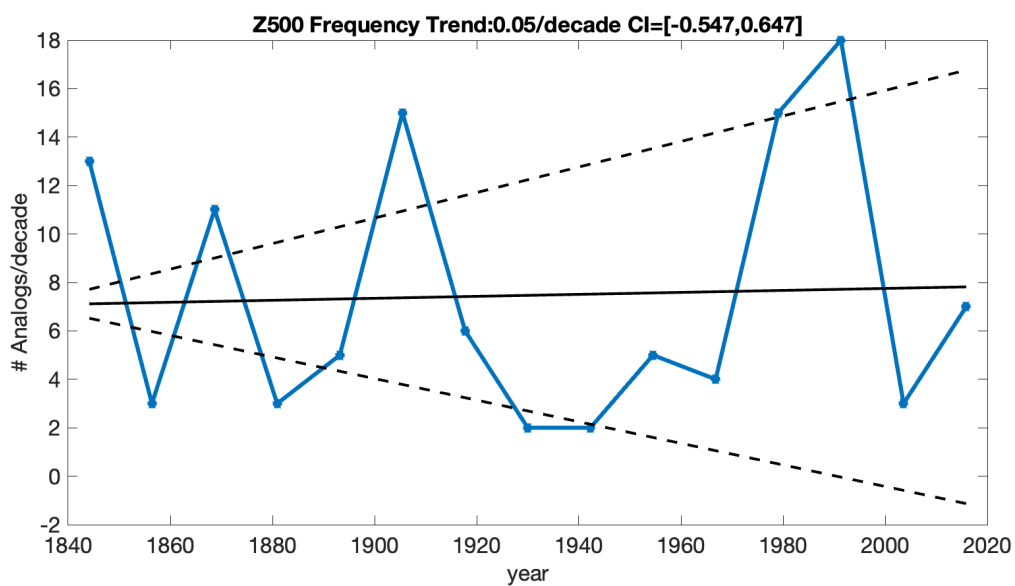


Figure S12. Evolution of the Frequency of analogs in time. As in Figure 3 in the main text, but for analogs of the non-bias corrected 500 geopotential height and the NCAR dataset.

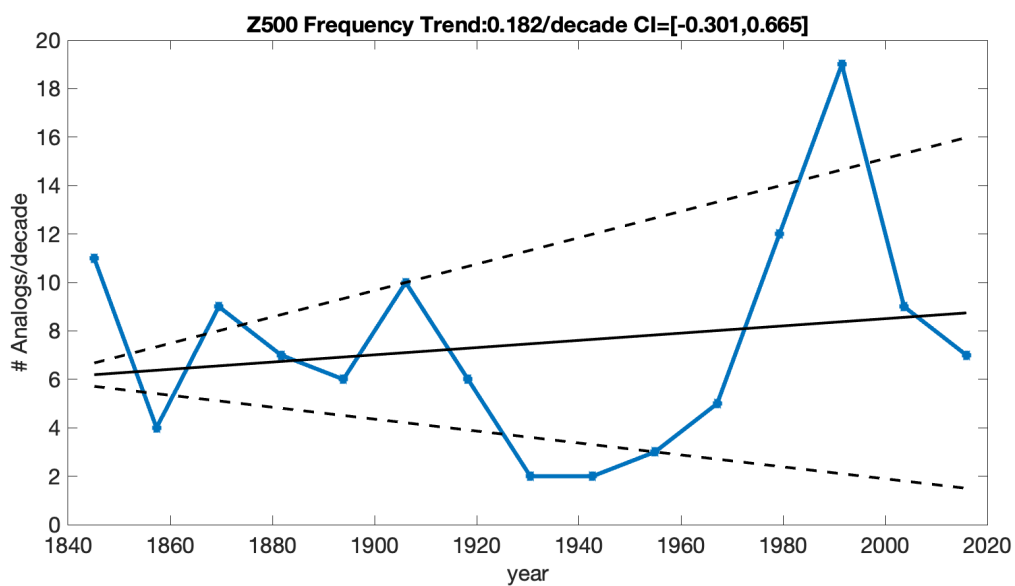


Figure S13. Evolution of the Frequency of analogs in time. As in Figure 3 in the main text, but for analogs of the bias corrected 500 geopotential height and the NCAR dataset.

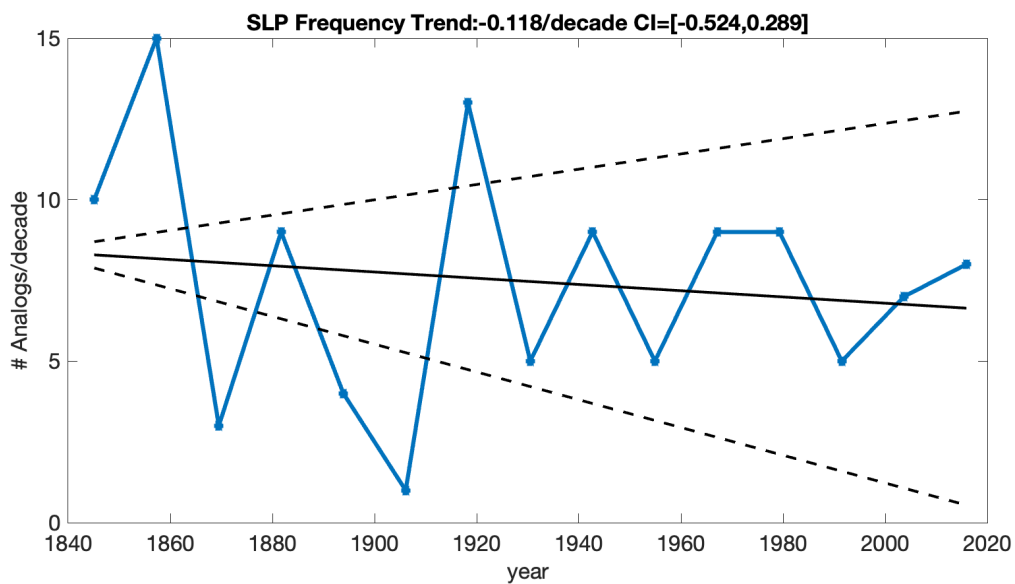


Figure S14. Evolution of the Frequency of analogs in time. As in Figure 3 in the main text, but for analogs of the bias corrected sea-level pressure and the DOE dataset.

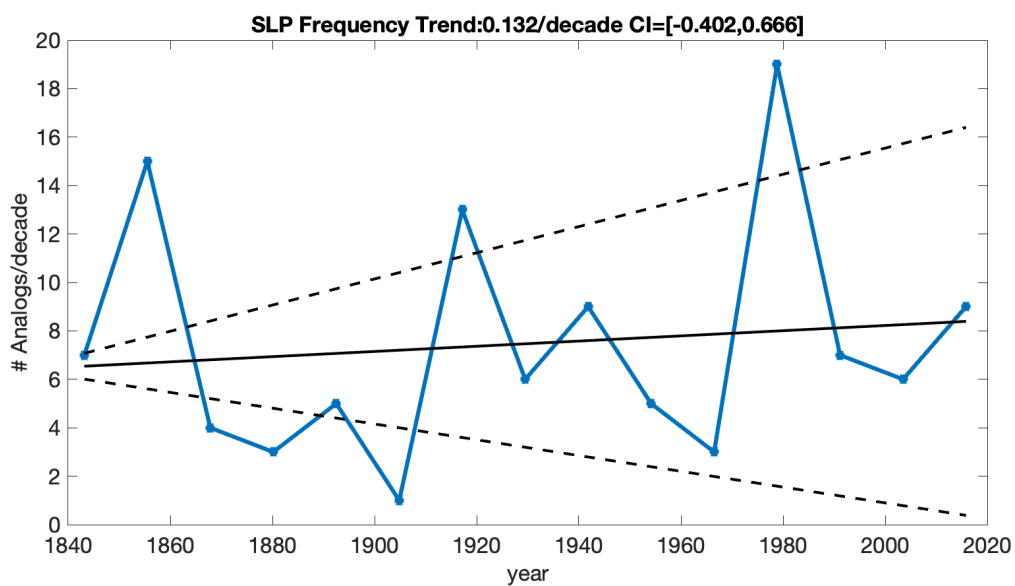


Figure S15. Evolution of the Frequency of analogs in time. As in Figure 3 in the main text, but for analogs of the non bias-corrected sea-level pressure and the DOE dataset.

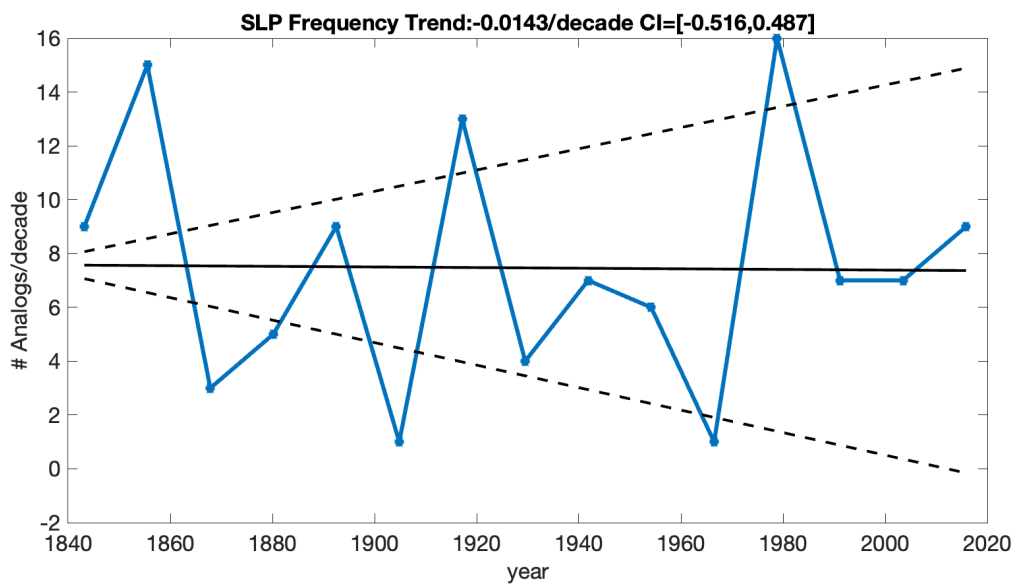


Figure S16. Evolution of the Frequency of analogs in time. As in Figure 3 in the main text, but for analogs of the bias corrected sea-level pressure and the NCAR dataset.

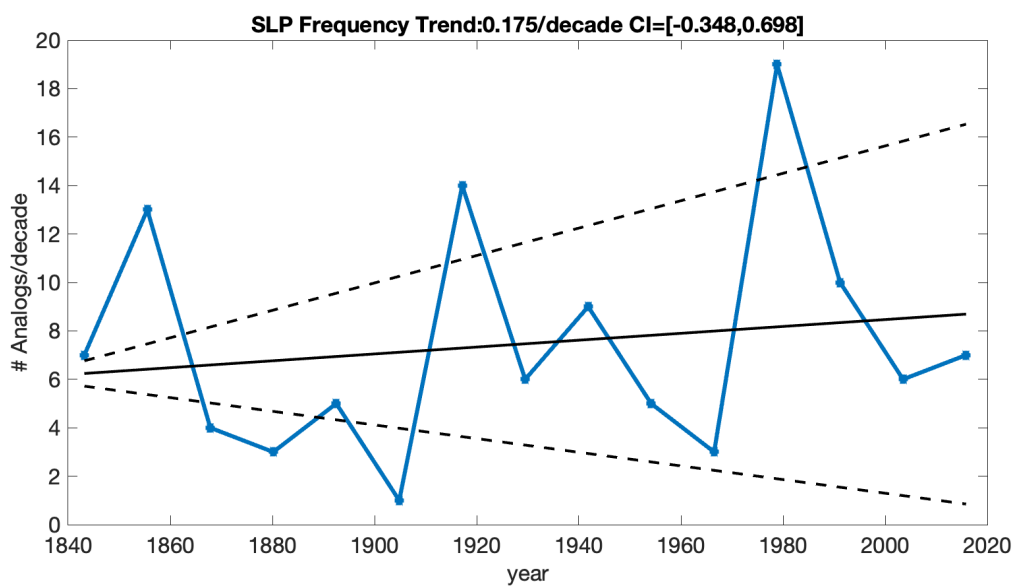


Figure S17. Evolution of the Frequency of analogs in time. As in Figure 3 in the main text, but for analogs of the non bias-corrected sea-level pressure and the NCAR dataset.

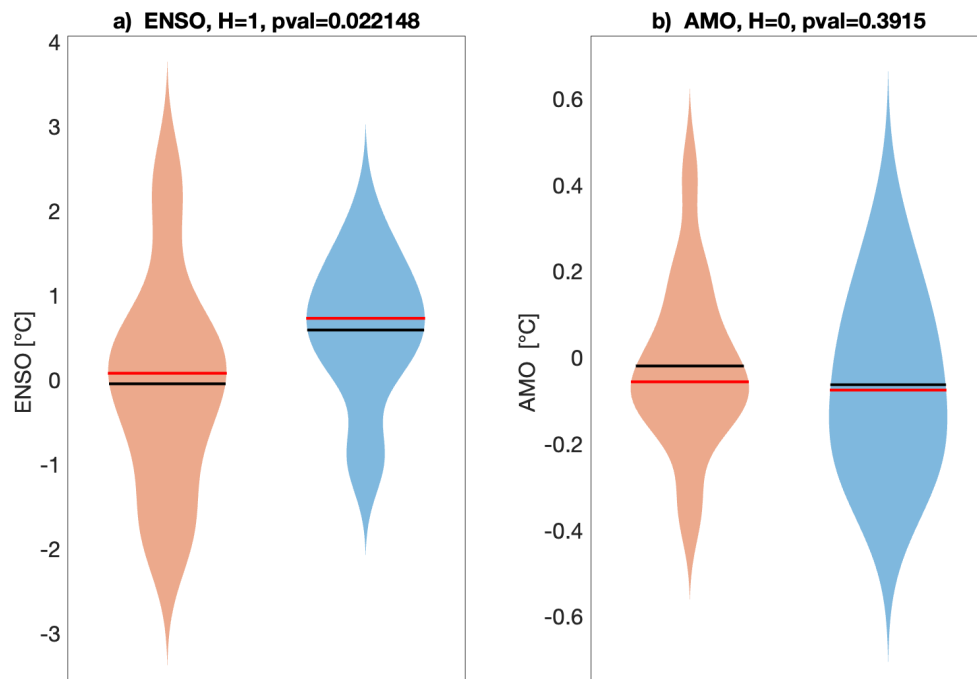


Figure S18. Analysis of the Interannual and Interdecadal variability. As in Figure 4 in the main text, but for analogs of the non-bias corrected 500 geopotential height and the DOE dataset.

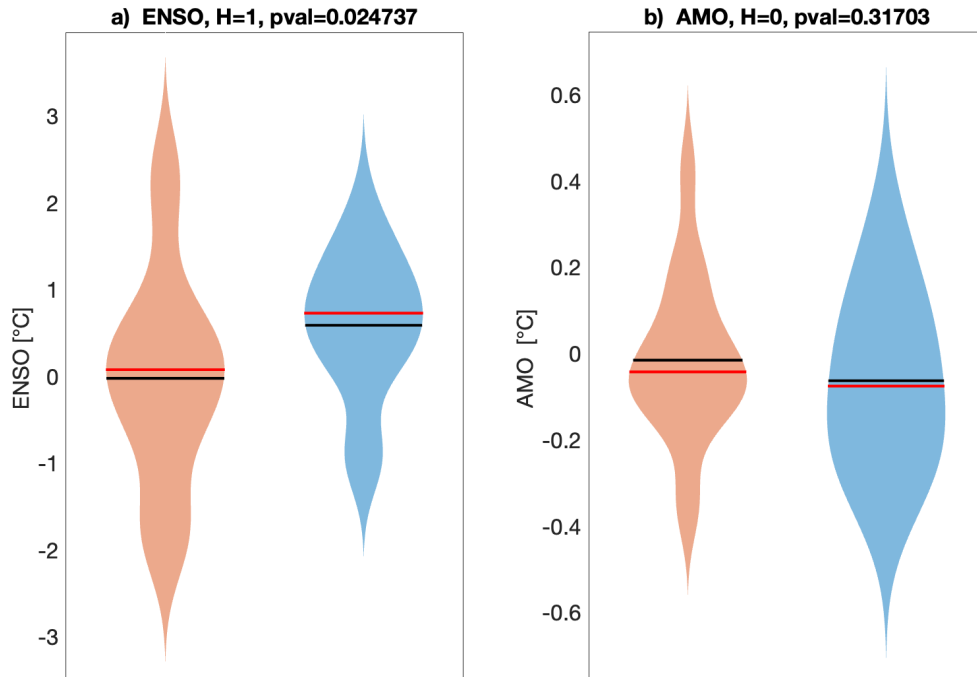


Figure S19. Analysis of the Interannual and Interdecadal variability. As in Figure 4 in the main text, but for analogs of the non-bias corrected 500 geopotential height and the NCAR dataset.

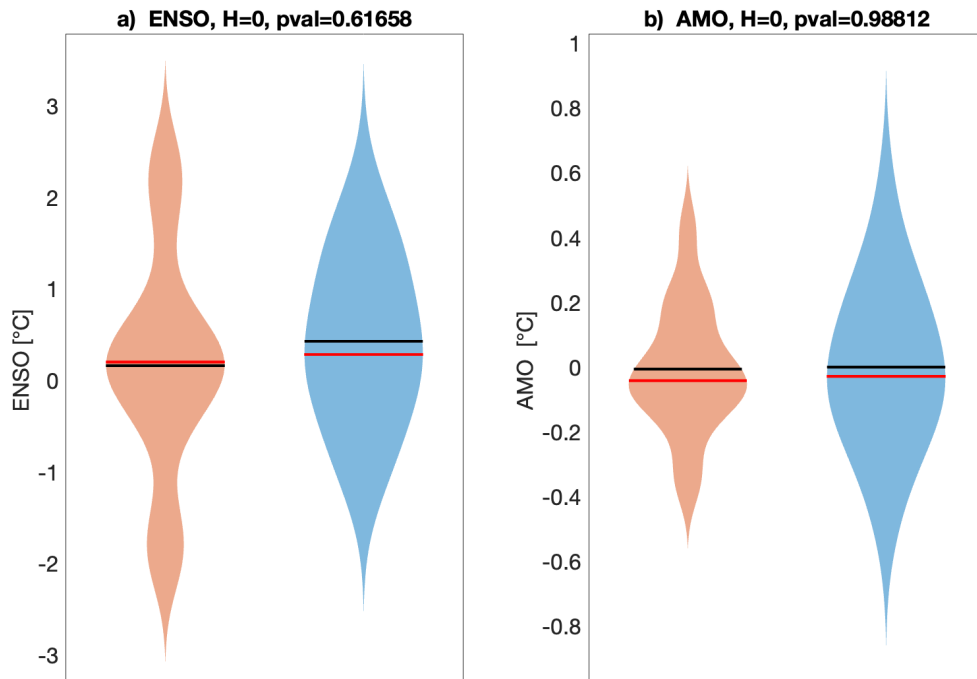


Figure S20. Analysis of the Interannual and Interdecadal variability. As in Figure 4 in the main text, but for analogs of the bias corrected 500 geopotential height and the NCAR dataset.

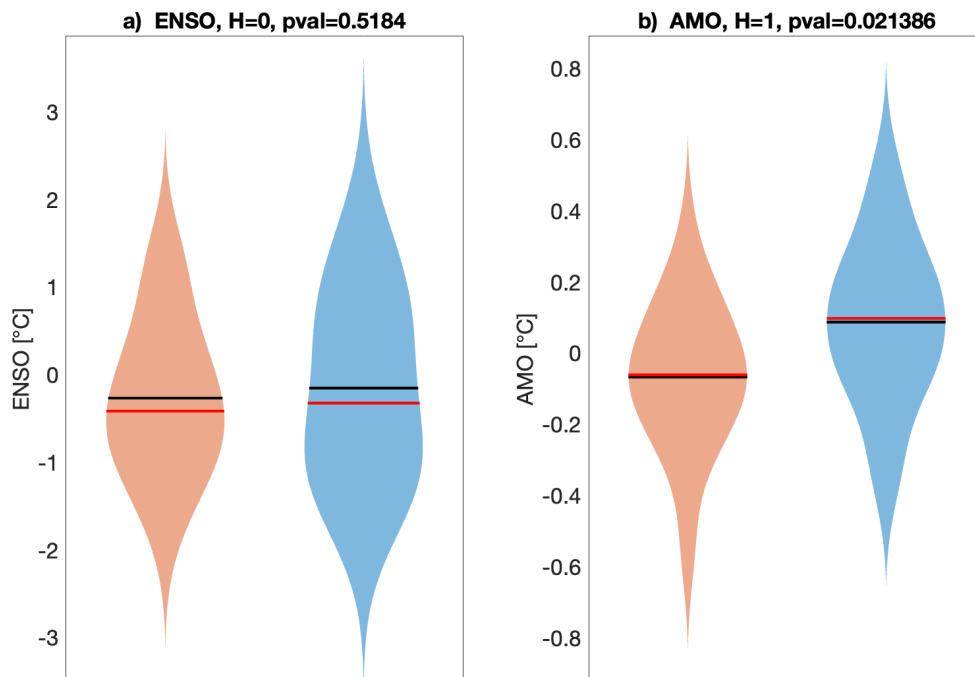


Figure S21. Analysis of the Interannual and Interdecadal variability. As in Figure 4 in the main text, but for analogs of the bias corrected sea-level pressure and the DOE dataset.

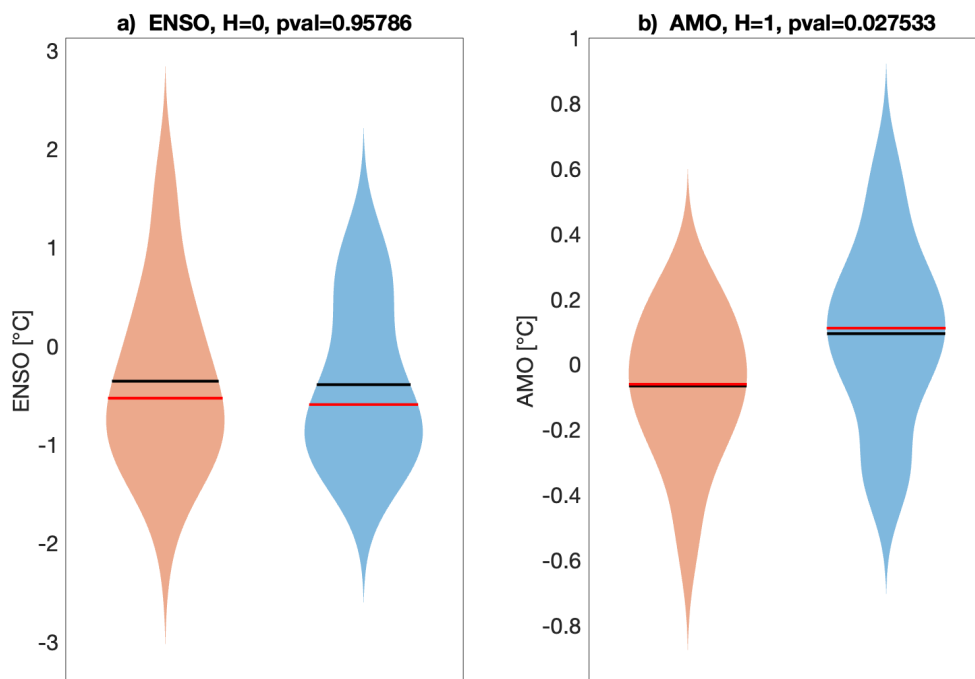


Figure S22. Analysis of the Interannual and Interdecadal variability. As in Figure 4 in the main text, but for analogs of the non bias-corrected sea-level pressure and the DOE dataset.

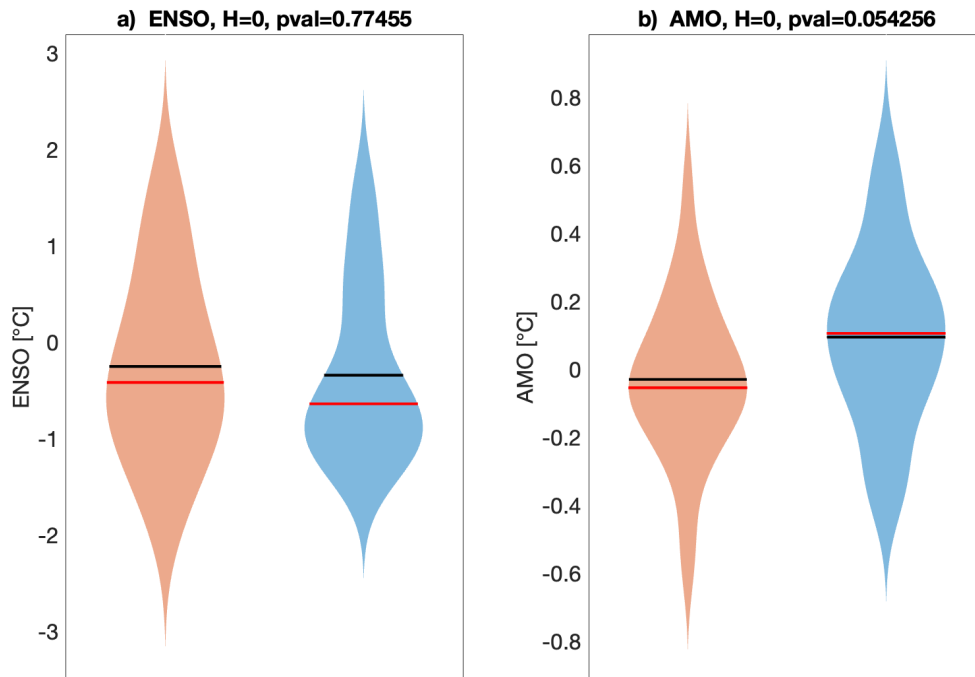


Figure S23. Analysis of the Interannual and Interdecadal variability. As in Figure 4 in the main text, but for analogs of the bias corrected sea-level pressure and the NCAR dataset.

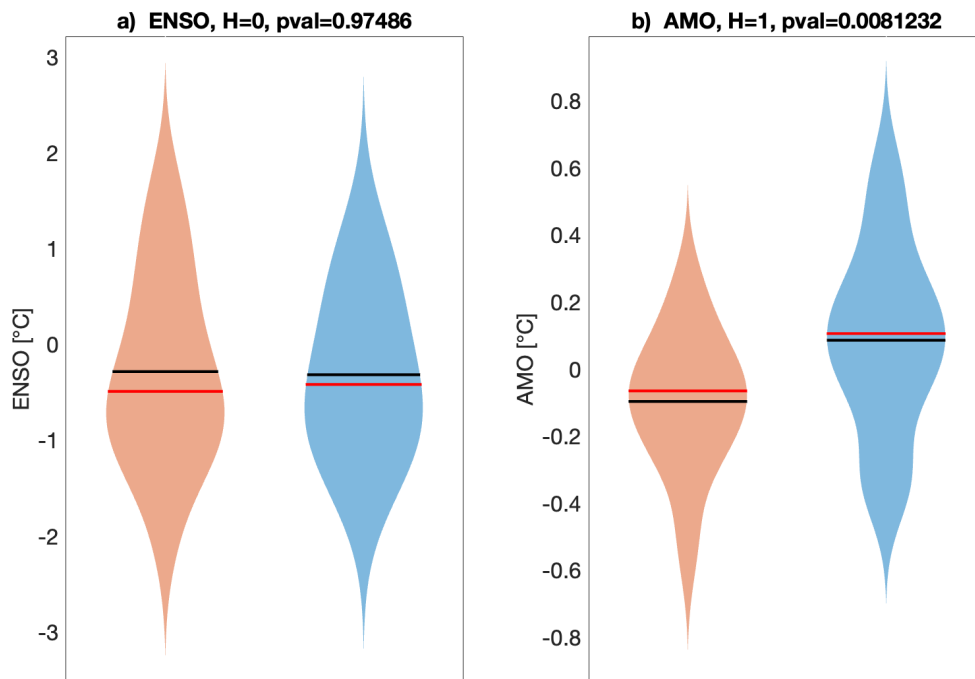


Figure S24. Analysis of the Interannual and Interdecadal variability. As in Figure 4 in the main text, but for analogs of the non bias-corrected sea-level pressure and the NCAR dataset.